A RADIATION MODEL OF A RAPID THERMAL PROCESSING SYSTEM

by

ABIGAIL WACHER

B.Sc., Simon Fraser University, 1997

A THESIS SUBMITTED IN PARTIAL FULFILLMENT OF
THE REQUIREMENTS FOR THE DEGREE OF

MASTER OF SCIENCE

in

THE FACULTY OF GRADUATE STUDIES

INSTITUTE OF APPLIED MATHEMATICS

DEPARTMENT OF MATHEMATICS

We accept this thesis as conforming
to the required standard

THE UNIVERSITY OF BRITISH COLUMBIA

February 2001

In presenting this thesis in partial fulfilment of the requirements
for an advanced degree at the University of British Columbia, I
agree that the Library shall make it freely available for reference
and study. I further agree that permission for extensive copying of
this thesis for scholarly purposes may be granted by the head of my
department or by his or her representatives. It is understood that
copying or publication of this thesis for financial gain shall not
be allowed without my written permission.

Department of _Mathematics_

The University of British Columbia
Vancouver, Canada

Date _May 8, 2001_

Abstract

In this thesis we study the radiative heat transfer that takes place in the axially symmetric Vortek rapid thermal processing chamber. A radiation model is derived using the theory of Shape Factors which we use to predict how chamber geometry and materials affect temperature uniformity on the processed silicon wafer. Using a series of numerical experiments on an axially symmetric domain we are able to predict the radiative effects on the temperature uniformity of the processed wafer in terms of the size of the showerhead and guard ring, the reflectivity of the showerhead and the chamber height.

$\jmath$

Table of Contents

Acknowledgments

I would like to thank Brian Seymour for his consistent support throughout my research and for his guidance during difficult times. Carl Ollivier-Gooch and myself spent many hours discussing the fluid dynamics and modeling required for my thesis which was very helpful in developing my research. I am thankful to Marcel Lefrancois for his help and suggestions which helped me understand the Vortek problem and data. Huaxiong Huang was also very helpful during the first stages of the project. Finally, I would like to thank my mother Yvonne Solorio and Big Byrd for their support during stressful times.

1 Introduction

The Vancouver based company Vortek is currently developing Rapid Thermal Processing (RTP) tools for semiconductor device processing. Inside the RTP chamber is a silicon wafer which is heated to hundreds of degrees Celsius in a few seconds. The main heat transfer that takes place in the Rapid Thermal Process is radiation, which is the main focus of this thesis. A model will be derived which enables the prediction of how chamber geometry and materials affect temperature uniformity on the processed silicon wafer. This chapter is an overview of the general structure of this thesis.

The second chapter begins with some preliminary definitions such as the definition of a semiconductor, followed by what impurities are and how they are related to semiconductors. Following is a description of RTP technology, how it applies to semiconductor processing and what the market demands on the RTP technology are. The second section is dedicated to the historical background of RTP including some important events regarding to the development of the technology. This chapter also introduces the Vortek black chamber, describes the most important characteristics considered in the model of this thesis and how the model will be used to achieve the temperature uniformity required by market demand.

The third chapter is an overview of the physics included in the model. Here we define the three types of heat transfer that are needed to understand the physical processes studied. We introduce the geometry of the Vortek chamber discussing the relative importance of the physics being considered and describe the details and values of the Vortek RTP chamber and process. Some of the important physical aspects discussed in this chapter are: the cooling gas, conduction and convection in the gas, recirculation cells, how the radiation from the lamp is absorbed and reflected, why conduction is included in the model, what the chamber wall materials are and how they are included in the model. Finally we describe the necessary simplification and assumptions that are made to make the study possible.

The intention of Chapter Four is to explain how the radiation is modeled to study the temperature uniformity of the wafer. First we define some of the vocabulary necessary to understand the equations that will be given throughout this chapter which include: emissive power, radiosity, irradiation, absorptivity, reflectivity and transmissivity. We define the equations that describe the radiant heat exchange between two parallel surfaces separated by a transparent media. We then derive the heat balance equation at the wafer surface and arrive at an implicit equation that relates temperature to time. In the final section Newton's method is applied to the heat balance equation in order to solve for temperature numerically at an instant in time and in this way advance the temperature in time at the wafer boundary.

Chapter Five discusses the numerical results obtained from following the model guidelines described in this thesis. This chapter includes discussions of: the drop off of temperature from the center to the edge of the wafer at peak temperatures, the effects of varying guard ring widths and showerhead

diameters, the effects of varying the chamber height and the effects of varying the showerhead reflectivities.

In Chapter Six we make recommendations for RTP design based on the results shown in Chapter Six and we conclude with some suggested future work.

Appendix A has the necessary background information on Shape Factors that is required for solving the heat balance equation discussed in chapter 5. In this appendix we derive a numeric formula for calculating the fraction of radiant energy leaving a (ring shaped)surface A_1 that is incident on a parallel (ring shaped) surface A_2. The material in this appendix has been extracted from Krieth (1962) and Chapman (1967).

Appendix B explains how the system of equations derived from the heat exchange between the wafer surface and the showerhead surface is solved to obtain the total irradiation at the surface of the wafer.

Appendix C describes an axially symmetric fluid model of the RTP chamber. Here we derive the equations for a uniform fluid and also define the equations of state for the perfect gas considered in this model. Since the domain considered is axially symmetric, we define a cylindrical coordinate system and use this to rewrite the equations in order to take advantage of the simplifications resultant of the axially symmetric assumption. The third section is dedicated to the non-dimensionalization of the axially symmetric equations. The fourth section rewrites the non-dimensional equations in vector form as required for the CFD model and develops a non-dimensional analysis of the parameters characteristic of these equations. The last section discusses the boundary conditions necessary for the model. For the model six different boundary conditions are needed. These are: Fixed Temperature, Wall Boundaries, Symmetry Boundaries, Inflow Boundaries, Outflow Boundaries and Radiation Boundaries. Most of these amount to specifying a constraint on the solution at the boundary of the computational domain derived from the continuity and momentum equations.

Appendix D contains information about silicon and nitrogen that were needed to do the present study of temperature on the silicon wafer which includes data tables and classical physical laws.

1.1 Model approach

This section is a brief overview of the model approach that has been taken to do the present study also naming the methods and programs that are used for studying the model.

My approach has been to develop a radiation model that predicts the temperature profile on the wafer during a process run with no gas flowing inside the Vortek chamber. Given that we know the irradiation from below the wafer and that the temperature at the showerhead is held constant we can calculate the temperature on the wafer (and guard ring) using a heat balance equation at the wafer (and guard ring) in conjunction with the radiative heat exchange between the wafer and the showerhead which is derived from Shape/View factor theory. The radiative heat exchange is modeled using shape factors resulting in a system of linear equations with irradiations as the unknowns. The linear

system of equations is solved using a classic LU decomposition with partial pivoting called Crout's method. Once the linear system of equations been solved the information is inserted into a heat balance equation. The heat balance equation is then solved analytically to obtain an explicit equation which is a function of temperature and time step. The explicit equation is then solved numerically using Newton's method to obtain a temperature after one step in time.

reflective grid

N$_2$

shower head

silicon wafer

guard ring

**98% absorbing
black chamber
wall**

quartz window

reflector
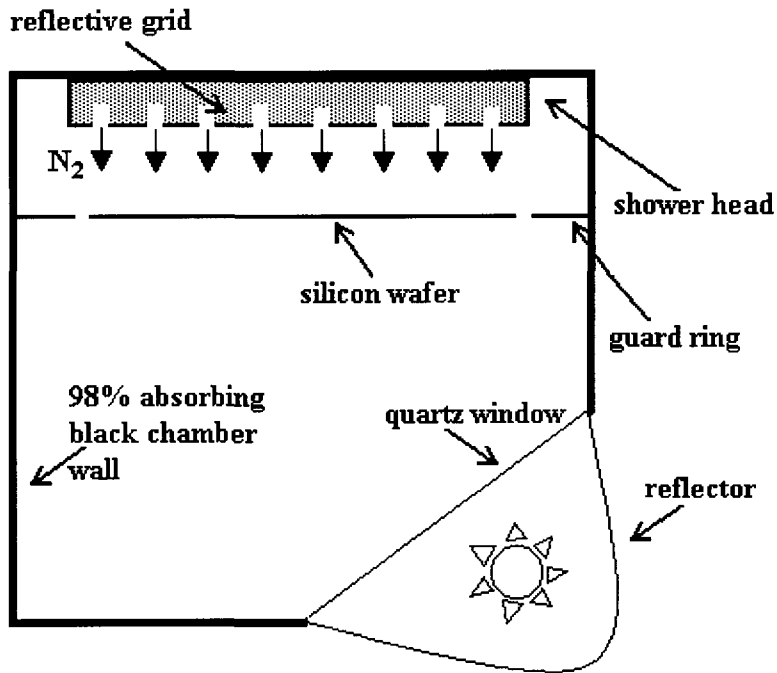
Figure 1: Vortek chamber

2   Background

In the following chapter I propose to motivate the reader by giving some preliminary definitions in the first section beginning with the definition of a semiconductor, followed by what impurities are and how they are related to semiconductors. After these definitions is a description of RTP technology, how it applies to semiconductor processing and what the market demands on the RTP technology are. The second section is dedicated to the historical background of RTP beginning with a definition of Rapid Thermal Processing as it is known in industry followed by some important events leading to the development of the RTP technology. The last section introduces the Vortek RTP tool, describes the most important characteristics considered in the model of this thesis and finally how the model will be used to make suggestions on how the temperature uniformity required by market demand may be achieved.

2.1 Definitions and Terminology

RTP processes silicon wafers to make semiconductors for computer devices and high speed computation applications. A semiconductor is a material having an electrical conductivity intermediate between that of metals which are always good conductors and insulators which are always poor conductors. Two common semiconductor materials are silicon and germanium. Semiconductor materials have an electrical conductivity which varies over many orders of magnitude ranging from about $10^{-9}/ohm\ cm$ to $10^3/ohm\ cm$. These variations in many cases depend on crystal imperfections which may be lattice defects or atoms incorporated into the crystal lattice with the addition of slight concentrations of impurities called dopants. The impurities added to the semiconductor when it is fabricated have a strong influence on the relative concentrations of the positive and negative charge carriers known as holes and electrons.

Impurities, or dopants, can be of two classes: Donor impurities or Acceptor impurities. Donor impurities are elements that have five valence electrons rather than the four that characterize silicon or germanium. Some common donor impurities used in semiconductor devices are phosphorus, arsenic and antimony. Since the donor impurities have five valence electrons rather than four, one valence electron is left over after the covalent bonds are formed and in the temperature range in which semiconductor devices commonly operate, the extra electron moves about the semiconductor as a conduction electron. Consequently donor impurities contribute conduction electrons to the semiconductor. Acceptor impurities are elements that have three valence electrons rather than the four that characterize silicon and germanium. Some acceptor impurities include boron, indium and aluminum. These atoms have one valence electron less than required to complete the covalent bonds. This vacancy in the bond structure is called a hole. At normal temperatures the hole becomes dissociated from the acceptor atom and is free to move throughout the semiconductor.

If a semiconductor contains a significant quantity of donor atoms, it has more electrons than holes and is known as an n-type semiconductor (n corresponds to the negative charge carrier). If however there is a significant quantity of acceptor atoms, the material is known as a p-type semiconductor (positive). Both the n-type and p-type semiconductors are called extrinsic because their electrical properties are governed by the impurities rather than by the semiconductor itself. If on the other hand a semiconductor contains negligible quantities of either acceptor or donor impurities, then the semiconductor is called intrinsic because its electrical properties are governed more by the semiconductor material itself rather than by the impurities.

Annealing is a process used to add impurities to the semiconductor by the method of thermally-activated diffusion. Rapid thermal processing (RTP) is one technology for thermally-activated diffusion. RTP heats a silicon wafer from room temperature to hundreds of degrees Celsius in a few seconds, holds the wafer a few seconds at the process temperature and then cools it rapidly. Temperature uniformity of the wafer during the annealing process is important to obtain uniform conductivity and resistivity throughout the wafer. The RTP

5

method has two advantages over conventional furnace annealing: RTP lowers the thermal budget (integral of time and temperature) and produces superior oxides and silicides.

The integrated (IC) market demands greater memory capacity, faster processing speeds and smaller device sizes for computer and high speed communication applications. Due to these demands there is a corresponding need to improve the semiconductor products resulting in tighter temperature uniformity requirements. The current uniformity requirements at the processing temperature of 1050°C is ±3 °C (3σ). "This assumes that measurement errors and real values fluctuate randomly. So when you measure a large sampling of wafers (10-100) it is expected that virtually all points are within 3 standard deviations of the mean, which means that 99% of the measured temperatures are within 3 °C of the mean 1050°C. The temperature uniformity is expected to be ±2 °C (3σ) in the year 2001 due to market demand," Lefrancois (2001).

2.2 Historical background of RTP

In 1999, at the 7th International Conference on Advanced Thermal Processing of Semiconductors, B. Lojek submitted a review of early RTP development. As Lojek (1999) describes in his paper: "Early History of Rapid Thermal Processing" there is no common agreement on the definition of Rapid Thermal Processing. Usually RTP is understood to mean:

- Single wafer processing

- Processing with shorter processing times in comparison to conventional batch furnaces

- Processing with fast heating and cooling rates

- Wafer is thermally isolated from processing chamber

- Cold wall and controlled ambient processing

- Processing with control of thermally driven surface reactions

"The most important difference between conventional batch thermal processing and Rapid Thermal Processing is the fact that in an RTP system the processed wafer is never in thermal equilibrium with the surrounding environment," Lojek (1999). There have been various different terms used to describe this process until Rapid Thermal Processing became the common term. In 1968 the term "rapid" was first used by Walter K. Mammel of Western Electric Company in New York in his patent: Patent #3,627,590 titled "Method of Heat Treatment of Work pieces" which defines all of the requirements of a state-of-the-art RTP system. The company Varian used the term Isothermal Annealing, AG Associates used "Heat Pulse Annealing", and in the academic world it was know as "Blink Furnace Annealing".

The origin of many RTP principles came from experiments in materials science. These include experiments which required the controlled heating and cooling of a material sample to understand "annealing" and its effects on material properties. A system designed in 1957 which resembles RTP was developed by a group of scientists at the California Institute of Technology in Pasadena, "A solar furnace with parabolic aluminum reflector", Hiester (1957). Another early RTP system: "was built by Naval Research Laboratory at the beginning of the 60's. In May 10, 1961 F.J. White presented at 1961 SESA Spring Meeting held in Philadelphia results of simulation of the conversion of mechanical energy into thermal energy to produce aerodynamic heating," Lojek (1999). The major issue of RTP which remains today is the temperature measurement of the processing sample, however in these earlier stages this was done by a thermocouple attached to the sample. "One of the problems with thermocouple is that they cannot be attached to a process wafer especially since some RTP chambers rotate the wafer. There are problems between process and monitor wafers as well," Lefrancois (2001). The first commercially available RTP annealing system using incoherent radiation corresponding to the black body temperature ($\sim 1450°C$) was the Extrion IA 200. Ron Fulks from the company Varian and Carl Russo from the company Extrion drove the project which resulted in "the Extrion IA-200 (Isothermal Annealer), introduced at Semicon-West in May 1981", Lojek (1999). For various reasons the IA-200 was not a commercial success.

Temperature measurement in the first RTP system was based on the optical pyrometer. Sato (1967) characterized emissivity of ultra pure optically polished silicon as a function of temperature. Sato's data was used to adjust the pyrometer. There are problems with the pyrometer, mainly due to the fact that the semiconductor subtrate used in semiconductor manufacturing is not the ultra pure material described by Sato in his paper. The thermocouple is still the most accurate temperature measurement device. However, it requires experience and is very expensive. As a consequence most of the work describing diffusion behaviour of semiconductors is accompanied by the uncertainty of the temperature of the sample.

2.3 Vortek

The RTP system studied in this thesis was designed by the Vancouver based company Vortek. Vortek Industries Limited was founded in 1976 as a spin-off company from the University of British Columbia. Dr. David M. Camm and other postgraduates of the physics department founded the company. "The first publication on the black chamber is David Camm and B.Lojek at the international conference on advanced thermal processing of semiconductors RTP' 94," Lefrancois (2001). On August 30, 1994 David M. Camm filed a patent application (# 5,561,735) in the United states, titled "Rapid Thermal Processing Apparatus and Method", Camm (1996). The patent describes an apparatus and method for rapidly and uniformly heating a workpiece. "The Vortek lamp is considered by many as the most suitable source of radiation for annealing of

Si implanted layer", Lojek (1999). The products and services as described by
Dr. Marcel Lefrancois (2001), the Senior Research Scientist at Vortek:

> The company developed the world's most powerful light. Vortek
> lamps are the results of years of development and operate between 50 and
> 300kW. Currently, Vortek markets high power arc lamps and material-
> processing systems based on these lamps. The systems are sold to R&D
> and manufacturing customers around the world. The R&D systems are
> used to simulate solar radiation over large areas or provide very intense
> heat sources. Applications include aerospace and scientific testing, sil-
> icon powder processing, thermal wave imaging, and contaminated waste
> processing. Vortek also manufactures a Rapid Thermal Processor (RTP)
> for solar cell manufacturing. This is used for dopant drive in and oxida-
> tion of the cells. The solar application shares common technology with
> semiconductor IC tools that Vortek is currently developing.

Vortek is currently developing a semiconductor tool that will be marketed
worldwide and built in B.C. The market potential for Vortek is in excess of
US$100 million (total market by 2005 is expected to be over US$500 million).

A simple schematic of the Vortek Black Chamber RTP unit is shown in
Figure 1. Light shines from a 200kW arc lamp through a quartz window onto
a wafer. The wafer is in a chamber with cold walls. The intensity required to
keep the wafer at 1050°C is approximately 35 W/cm^2 when there is gas flowing
in from a showerhead as in Figure 1. The radiation exchange between the
wafer and the chamber surfaces is the main thing which affects the temperature
uniformity and will be studied in this thesis. The gas can carry away about 1-2
W/cm^2 from the wafer surface. This corresponds with a temperature change
of about 3°C when the energy delivered to the wafer changes by 0.3 W/cm^2.
Suggestions on flow profiles will be included in the thesis in consideration of this.
In the present thesis, a model is developed for predicting the temperature profile
on the wafer inside the Vortek chamber. The model focuses on the radiation
exchange between the wafer and the reflecting surface above it and studies how
changes in chamber geometry and materials affect the temperature uniformity
of the wafer. It is recommended as future work to model the gas flows in the
chamber throughout a short process run in order to make the wafer temperature
more uniform, and so in appendix C a fluid model has been outlined and there
it is described how to couple the model of this thesis as a boundary condition
with the fluid model. Because the same underlying principles apply to any RTP
chamber regardless of geometry, much will be learned by studying the simple
geometry of the existing chamber and the model should be easy to apply to
different chamber configurations and chamber materials in order to maximize
temperature uniformity inside the chamber.

3 Heat Transfer and Geometry

This chapter is an overview of the physics included in the model of the RTP process and why it is important to consider these. The first section of this chapter defines the three types of heat transfer that are needed to understand the physical processes included in the RTP process. The following section discusses the geometry of the Vortek RTP shown in Figure 2. The third section is intended to give the reader an understanding of the relative importance of the physical processes and is dedicated to the specific details and values of the Vortek RTP chamber and process. The fourth section discusses the cooling gas, conduction and convection in the gas, and when recirculation cells will appear in the flow profile. This section also discusses the chamber wall materials and how they are included in the model. The last section describes the necessary simplifications and assumptions that are made in this study.

3.1 Definitions

There are three basic types of heat transfer processes called conduction, convection and radiation. It is important here to define and understand these types of heat transfer in order to describe and analyze a rapid thermal processing system.

"Heat conduction is the term applied to the mechanism of internal energy exchange from one body to another, or from one part of a body to another part, by the exchange of the kinetic energy of motion of the molecules by direct communication or by the drift of free electrons in the case of heat conduction in metals," Chapman (1967). It is important to note that "conduction takes place within the boundaries of a body, or across the boundary of a body into another body placed in contact with the first," Chapman (1967).

"Convection is the term applied to the heat transfer mechanism which occurs in a fluid by the mixing of one portion of the fluid with another portion due to gross movements of the mass fluid, " Chapman (1967). Natural convection occurs when there is a temperature difference imposed on a fluid and is a result of the density difference in the fluid.

"Thermal radiation is the term used to describe the electromagnetic radiation which has been observed to be emitted at the surface of a body which has been thermally excited. This electromagnetic radiation is emitted in all directions; and when it strikes another body, part may be reflected, part may be transmitted, and part may be absorbed. If the incident radiation is thermal radiation, i.e. if it is of the proper wavelength, the absorbed radiation will appear as heat within the absorbing body," Chapman (1967).

3.2 Chamber geometry

The Vortek chamber shown in Figure 2 contains a thin silicon wafer placed so that it divides the chamber into two compartments. The upper compartment has a highly reflective metal grid (showerhead) above the wafer. Gas
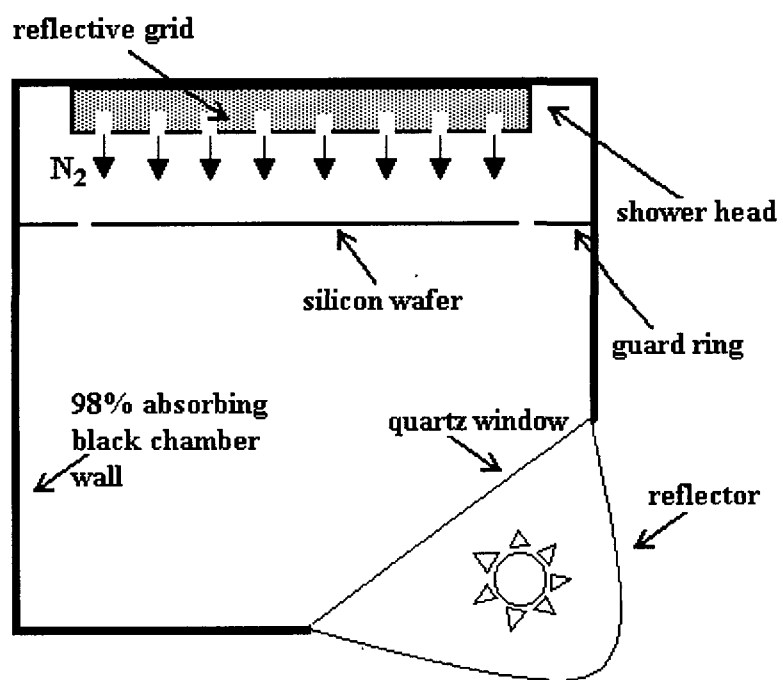
Figure 2: Vortek chamber

may be injected into the chamber using the shower head. The wafer has a guard ring (there is a small space between the wafer and the guard ring) that helps maximize the temperature uniformity on the wafer surface by blocking energy reflections from the chamber walls. "The guard also makes the wafer appear larger in reflections, therefore the gradient moves outward from wafer onto guard," Lefrancois (2001) The lower compartment is a black cavity, that absorbs all reflected radiation from the wafer, thus preventing it from reflecting back to the wafer. The radiation source is an intense arc lamp (Vortek's water-wall arc-lamp), mounted in a reflector so that the radiation reflected and emitted from the wafer is minimized and totally absorbed by the cavity walls. "Thus all secondary radiation is eliminated from the lower cavity," Lefrancois (2001).

3.3   Chamber specifications

Light shines from a (200 kW) arc lamp through a quartz window positioned in such a way that the light shines uniformly on the bottom surface of the silicon wafer. The wafer is typically 200mm in diameter and 0.7mm thick. It's total hemispherical emissivity is approximated to 0.68, which is the emissivity at temperatures above approximately 700°C obtained from Sato (1967). The wafer is heated from below from room temperature to a maximum temperature of 1050°C. A cooling gas (nitrogen) can be injected into the upper compartment from the shower head which is presently made of hand polished aluminum with a reflectivity of about 0.7. The showerhead is water cooled, and kept at a constant temperature of about room temperature to approximately 100°C. Note that the emissivity of the shower head is important and must be included. The gap between the shower head and the surface of the wafer is adjustable from 2 mm to 2 inches; at present it is set at 1 cm. The cooling gas is injected with a flow rate that may vary from zero upward, but a good value is 10 standard liters per minute (no preheating- but this is variable). The gas flows down and through the upper compartment and out of the chamber, upward through the outlet placed between the shower head and the chamber walls.

"The radiant flux required to maintain the maximum temperature is $33.6W/cm^2$ without the shower head in place. When the shower head is included but no gas flow, the flux required to reach the maximum temperature is $28.9W/cm^2$," Lefrancois (2001). Given the above specifications, the Vortek RTP is currently able to process silicon wafers so that at the peak mean temperature of 1050°C, the temperature uniformity is $\pm 3\,°C$ (3σ). As discussed in the introduction, the goal of this study is to maximize temperature uniformity, ideally to obtain a uniformity of $\pm 2\,°C$. (3σ) Through numerical variation of the chamber parameters such as the gap between that wafer and the reflective showerhead, it is hoped to improve uniformity results.

3.4 Physical processes involved

The physics that is considered in this model is the physics of heat and mass transfer, though the main effects studied here are those caused by the radiant heat exchange.

The fluid in direct contact with the hot wafer surface is heated up by conduction. This heating results in a temperature difference between the fluid in direct contact with the wafer and the more removed fluid. The temperature difference induces a flow of energy from the hot fluid to the cold fluid creating what is called a convective current. This flow carries some of the energy away from the hot wafer and is used to cool the upper surface of the wafer and aids in improving temperature uniformity. This type of cooling is called convective cooling.

When there is a large gap between the lower hot surface (wafer) and the cool upper surface (shower head) the flow will recirculate creating rolling cells of fluid, and in this case the heat transfer in the fluid will be dominated by convection. On the other hand if there is too small of a gap between the lower hot surface and the cool upper surface the heat transfer in the fluid will be dominated by conduction and recirculation cells will be less apparent.

The primary heating source is the Vortek arc lamp which heats the silicon wafer by radiation, which is the dominant mode of heat transfer in RTP. This is in contrast to a regular batch reactor where wafers are stacked a few milimeters apart and so convective and conductive heat transfer are dominant. The radiation from the lamp does not appreciably heat up the fluid between the lamp and the wafer due to the fact that the nitrogen in the chamber is transparent; this means that all of the radiation is transmitted through the fluid and none is absorbed or reflected. Due to the black walls on the lower cavity of the chamber and the position of the lamp, the only incident energy on the lower surface of the wafer will be the radiation directly from the lamp. The wafer absorbs this energy and then some is emitted through both the top and bottom surfaces of the wafer by radiation and conduction.

The radiative energy that is emitted on the lower surface of the wafer gets absorbed completely by the black walls and is never reflected back to the wafer surface. Most of the radiative energy that is emitted from the upper surface of the wafer strikes the surface of the shower head. Some of this energy is absorbed (30%) and the rest is reflected back to the wafer surface.

In addition to the radiative exchange some of the energy emitted from the wafer is conducted from the wafer surface (both upper and lower surfaces) into the fluid that is in direct contact with the wafer. Though the amount of heat transfer by conduction is small in comparison to the radiative exchange (especially when there is no flow) an approximation has been included in the physics of this model using a linear approximation for the temperature gradient.

The showerhead and the walls of the chamber have a cooling system installed inside the material. Any energy that is absorbed by the chambers inner surfaces is carried away by the interior cooling system and so maintaining all the walls and surfaces inside the chamber (with exception of the wafer) at a

low fixed temperature of approximately 100°C. "Our wall temperatures are low - but sometimes it is desirable to keep the walls above 100°C - this prevents condensation - and water can be absolutely disastrous in some processes - others like wet oxidation - forms water by reacting hydrogen and oxygen in the chamber - a condensation point would cause non-uniform application in the process chamber," Lefrancois (2001).

3.5   Physical assumptions

Some physical assumptions and geometry simplifications must be made to make this study possible given the time and tools available. Once these assumptions have been made one can define a computational domain. The following is a description of the simplified computational domain.

The light intensity from the lamp is assumed to be uniform at the wafer lower surface. The silicon wafer will be assumed infinitely thin in the sense that the temperature on the top surface of the wafer will be assumed identical to the temperature on the lower surface. The chamber has an axially symmetric geometry. A linear approximation is used for the temperature gradient at the bottom and top surfaces of the wafer. The cooled walls and the showerhead are assigned a fixed temperature boundary condition. The total hemispherical emissivity is approximated to 0.68, which is the emissivity at temperatures above approximately 700°C obtained from Sato (1967)

4 Radiation

The intention of this chapter is to derive a heat balance equation on the wafer in order to produce a temperature profile which varies in time during a process run with no flow inside the Vortek chamber. Defined in the first section are some of the vocabulary necessary to understand the equations that will be given throughout this chapter. These definitions include: emissive power, radiosity, irradiation, absorptivity, reflectivity and transmissivity. In the second section we define the equations that describe the radiant heat exchange between two parallel surfaces separated by a transparent medium. First the equations are defined for the two surfaces shown in Figure 3, and then the equations are derived for each of the surfaces split into an arbitrary finite number of pieces resulting in an equation for each piece of surface. In the third section we derive the heat balance equation for each corresponding surface and for each surface we arrive at an implicit equation that relates temperature to time. In the final section Newton's method is applied to the heat balance equation in order to solve for temperature numerically at an instant in time and in this way advance the temperature in time at the wafer.

4.1 Background

The following is a list of nomenclature that will be used in our formulations:

Quantity	Symbol	Si Units
Emissive power	W	W/m^2
Radiosity	J	W/m^2
Irradiation	G	W/m^2
Total hemispherical emissivity	ϵ	
Temperature	T	K
Absorptivity	α	
Reflectivity	r	
Transmissivity	τ	
Area	A	m^2
Mass density	ρ	kg/m^3
Heat capacity (Specific heat)	C_p	$J/(kg \cdot K)$
Thermal conductivity	k	$W/(m \cdot K)$
Shape factor	F_{12}	
Time	t	s
Time step (Change in time)	Δt	s
Thickness of silicon wafer	h_{Si}	m

Constant	Symbol	Value
Stefan-Boltzmann constant	σ	$5.67E-8 \ W/(m^2 \cdot K^4)$

"Thermal radiation is the term used to describe the electromagnetic radi-

ation which has been observed to be emitted at the surface of a body which has been thermally excited. This electromagnetic radiation is emitted in all directions; and when it strikes another body, part may be reflected, part may be transmitted, and part may be absorbed. If the incident radiation is thermal radiation, i.e. if it is of the proper wavelength, the absorbed radiation will appear as heat within the absorbing body," Chapman (1967). For a given surface we define:

W = Emissive power, i.e., Total emitted thermal radiation leaving a surface, per unit area. $W = \epsilon\sigma T^4$, where T is the given temperature of the surface, σ is the Stefan-Boltzmann constant and ϵ is the total hemispherical emissivity at that temperature. For a given temperature the emissivity ϵ may have a value between 0 and 1 and is characteristic of the material. Black surfaces have emissivity close to one and thus emit more radiation than shiny surfaces that have emissivity close to zero.

J = Radiosity, i.e., Total thermal radiation leaving the surface, per unit surface area. Radiosity includes the original emitted radiation plus the reflected radiation.

G = Irradiation, i.e., Total thermal radiation incident upon the surface per unit surface area and is the result of the emitted radiation and reflections from other surfaces.

The relation between the energy that is absorbed, reflected and transmitted by a material is given by the law of conservation of energy:

$$\alpha + r + \tau = 1 \tag{1}$$

where

α = absorptivity, i.e., the fraction of the incident radiation absorbed

r = reflectivity. i.e., the fraction of the incident radiation reflected

τ = transmissivity, i.e. the fraction of the incident radiation transmitted through the body.

Absorptivity, reflectivity and transmissivity are temperature dependant variables that also depend on the surface characteristics, structure, material, and the wavelength of the incident radiation. For each surface considered here α, r and τ will be taken as constants given that the surfaces are flat and opaque, and the incident radiation has a dominant wavelength. Since the surfaces are opaque,

15
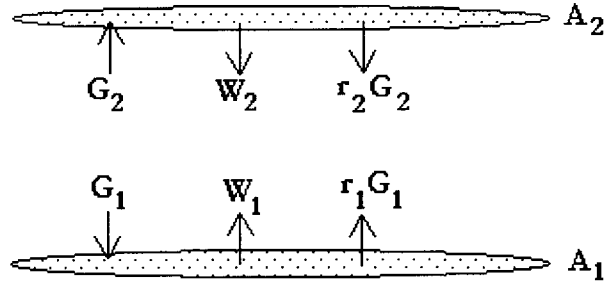
Figure 3: Radiation exchange between two parallel surfaces

$\tau = 0$, and so at each surface: $\alpha + r = 1$. In addition to this information we will need a corollary of Kirchhoff's law which states that at thermal equilibrium the absorptivity and the emissivity of any body are equal, or $\alpha = \epsilon$. This means that surfaces that emit less radiation, also absorb less of the radiation incident upon the surface and so most of the incident radiation is reflected. However darker surfaces with large emissivity absorb more of the incident radiation and thus are less reflective.

4.2   Radiation exchange equations

Assuming the space between the two parallel surfaces shown in Figure 3 is filled with nitrogen and assuming that the thermal radiation passes through it as though in a vacuum, then the transmissivity is 1, i.e., $\alpha = r = 0$. Further assume that surface A_2 is cooled so that it is maintained at a constant temperature. The equation for the total radiant energy leaving a surface is:

$$J = W + rG = W + (1 - \alpha)G \tag{2}$$

So for A_1 and A_2 where the gas is nitrogen, the heat exchange due to radiation can be described:

$$J_1 = W_1 + (1 - \epsilon_1)G_1 = \epsilon_1 \sigma T_1^4 + (1 - \epsilon_1)G_1 \tag{3}$$

$$J_2 = W_2 + (1 - \epsilon_2)G_2 = \epsilon_2 \sigma T_2^4 + (1 - \epsilon_2)G_2 \tag{4}$$

16
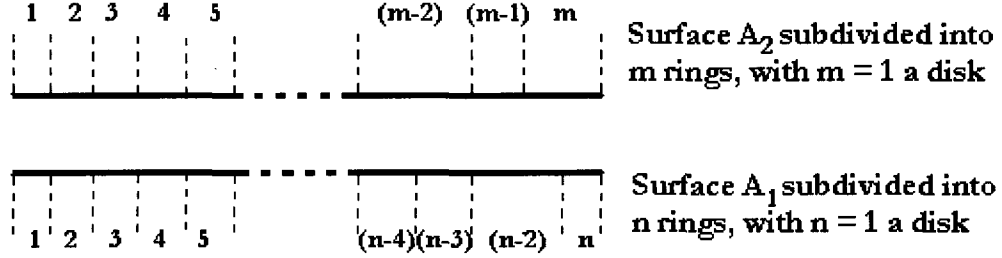
Figure 4: Subdivision of two disk shaped surfaces

The energy leaving surface A_2 which eventually strikes surface A_1 is given by: $A_2 F_{21} J_2$, where F_{12} is the shape factor based on area A_1.[1] G_1 is the radiant energy leaving surface A_2 which strikes A_1 per unit surface area, and is thus equal to: $\dfrac{A_2 F_{21} J_2}{A_1} = F_{12} J_2$. Applying the same principles at A_2 : G_2 is the radiant energy leaving surface A_1 which strikes A_2 per unit surface area, and is thus equal to $F_{21} J_1$, where F_{21} is the shape factor based on area A_2.

Inserting G_1 and G_2 into the Radiant energy equations results in two equations for two unknowns: J_1 and J_2:.

$$J_1 = \epsilon_1 \sigma T_1^4 + (1 - \epsilon_1) F_{12} J_2 \tag{5}$$

$$J_2 = \epsilon_2 \sigma T_2^4 + (1 - \epsilon_2) F_{21} J_1 \tag{6}$$

If further we subdivide each of A_1 and A_2 into a finite number of rings (not necessarily of equal width and each surface may be subdivided into a different number of rings) as in Figure 4. We then get the following formulae for the corresponding radiative system:

$$J_{1_i} = \epsilon_{1_i} \sigma T_{1_i}^4 + (1 - \epsilon_{1_i}) G_{1_i} \quad for \ i = 1..n \tag{7}$$

$$J_{2_j} = \epsilon_{2_j} \sigma T_{2_j}^4 + (1 - \epsilon_{2_j}) G_{2_j} \quad for \ j = 1..m. \tag{8}$$

---

[1]The definition of shape factor, and how to calculate it, is given in Appendix A. For further information on Shape Factor manipulation see Appendix A.

$\epsilon_{2j} = \epsilon_{showerhead}$ will be constant for all j. {Note, When the ring in consideration is an inflow, $\tau \neq 0$ as assumed above but rather $\tau = 1$, in which case $\alpha = 0, r = 0$, and thus at an inflow $J_{1_i} = 0$.}

$\epsilon_{1_i} = \epsilon_{silicon}$ will be constant for all i.

$\sigma =$ Stefan-Boltzmann constant $= 5.67051E - 8 \left(\dfrac{W}{m^2 K^4} \right)$

T_{2_j} will be constant for each j.

$T_{1_i} = T_{1_i}(t)$

If we replace G_{1_i} and G_{2_j} using the reciprocity and decomposition laws for Shape-Factors:

$$J_{1_i} = \epsilon_{1_i} \sigma T_{1_i}^4 + (1 - \epsilon_{1_i}) \sum_{j=1}^{m} F_{1_i 2_j} J_{2_j} \quad for \ i = 1..n. \tag{9}$$

$$J_{2_j} = \epsilon_{2_j} \sigma T_{2_j}^4 + (1 - \epsilon_{2_j}) \sum_{i=1}^{n} F_{2_j 1_i} J_{1_i} \quad for \ j = 1..m. \tag{10}$$

Note that $F_{2_j 1_i}, F_{1_i 2_j}$ will be constant for each i and each j.

The above is a system consisting of $(n + m)$ linear coupled equations and $(n + m)$ unknowns: $J_{1_1}, J_{1_2}, J_{1_3}, ...J_{1_n}, J_{2_1}, ...J_{2_m}$, for further details on how this linear system is solved the reader is referred to Appendix B.

4.3   Heat balance equation at the wafer

We will express the heat balance equation at the wafer using the coordinate system shown in Figure 6.

Given that we know (w.r.t. time) the irradiation from below surface A_1 (from the lamp) as in Figure 5, and that the temperature at surface A_2 is held constant, and assuming that A_1 (the silicon wafer) is infinitely thin, we may calculate at each step in time the temperature at surface A_1. This is achieved by looking at the radiative heat exchange between the two surfaces, solving for

18
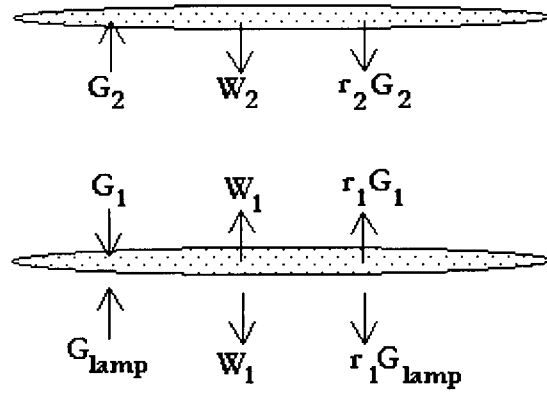
Figure 5: Radiation exchange including lamp
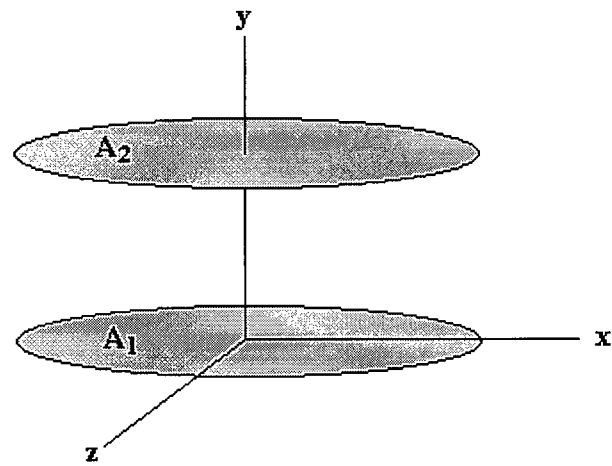
Figure 6: Coordinate system

the irradiation on each A_{1_i} (by solving the system given by Equations 9 and 10) and advancing the temperature at each A_{1_i} in time by using the following heat balance equation at A_{1_i}; where h_{Si} is the thickness of wafer , ρ_{Si} is the density of silicon, $C_{p_{Si}}$ is the Heat capacity of silicon, k_{Ni} is the conductivity of nitrogen.

$$\rho_{Si} C_{p_{Si}} h_{Si} \frac{\partial T_{1_i}}{\partial t} = G_{1_1} + G_{lamp} - 2W_{1_i} - r_{1_i} G_{1_i} - r_{1_i} G_{lamp}$$

$$-k_{Ni} \frac{\partial T_{1_i}}{\partial y}\bigg|_{aw} - k_{Ni} \frac{\partial T_{1_i}}{\partial y}\bigg|_{bw} \quad for \ i = 1..n$$

(11)

The first term on the left hand side of the equation represents the change of energy of A_{1_i} with respect to time. On the right hand side of the equation are the seven terms representing the incoming and outgoing energy at A_{1_i}. The positive terms represent the incoming energy and the negative terms represent the outgoing energy. The first term G_{1_1} is the total thermal radiation incident on A_{1_i} from above, per unit surface area. G_{lamp} is the total thermal radiation incident on A_{1_i} from the lamp below, per unit surface area. W_{1_i} is the total emitted thermal radiation leaving each side (surface) of A_{1_i} per unit area, and so this term is included twice. $r_{1_i} G_{1_i}$ is the total thermal radiation reflected at the top surface of A_{1_i}, per unit surface area. $r_{1_i} G_{lamp}$ is the total thermal radiation reflected at the bottom surface of A_{1_i}, per unit surface area. $\frac{\partial T_{1_i}}{\partial y}\bigg|_{aw}$ is the temperature gradient above the wafer at A_{1_i} and $\frac{\partial T_{1_i}}{\partial y}\bigg|_{bw}$ is the temperature gradient below the wafer at A_{1_i}. The values used for h_{Si}, ρ_{Si}, $C_{p_{Si}}$, k_{Ni}, $\frac{\partial T_{1_i}}{\partial y}\bigg|_{aw}$ and $\frac{\partial T_{1_i}}{\partial y}\bigg|_{bw}$ are given in Appendix D.

Replacing r_{1_i} with $(1 - \epsilon_{1_i})$, W_{1_i} with $\epsilon_{1_i} \sigma T_{1_i}^4$ and G_{1_i} with $\sum_{j=1}^{m} F_{1_i 2_j} J_{2_j}$ we get the following simplified equation:

$$\rho_{Si} C_{p_{Si}} h_{Si} \frac{\partial T_{1_i}}{\partial t} = \epsilon_{1_i} \sum_{j=1}^{m} F_{1_i 2_j} J_{2_j} + \epsilon_{1_i} G_{lamp} - 2\epsilon_{1_i} \sigma T_{1_i}^4$$

$$-k_{Ni} \frac{\partial T_{1_i}}{\partial y}\bigg|_{aw} - k_{Ni} \frac{\partial T_{1_i}}{\partial y}\bigg|_{bw} \quad for \ i = 1..n$$

(12)

We may rewrite this as:

$$\frac{\partial T_{1_i}}{\partial t} = \frac{-2\epsilon_{1_i}\sigma}{\rho_{\text{Si}}C_{p_{\text{Si}}}h_{\text{Si}}} \times$$

$$\left(T_{1_i}^4 - \frac{1}{2\epsilon_{1_i}\sigma}\left(\epsilon_{1_i}\sum_{j=1}^m F_{1_i 2_j}J_{2_j} + \epsilon_{1_i}G_{lamp} - k_{Ni}\left.\frac{\partial T_{1_i}}{\partial y}\right|_{aw} - k_{Ni}\left.\frac{\partial T_{1_i}}{\partial y}\right|_{bw}\right)\right) \tag{13}$$

Using the information from the previous time step, for each i and j we have:

$$\epsilon_{1_i}, \ \rho_{\text{Si}}, \ C_{p_{\text{Si}}}, \ F_{1_i 2_j}, \ J_{2_j}, \ G_{lamp}, \ k_{Ni}, \ \left.\frac{\partial T_{1_i}}{\partial y}\right|_{aw}, \ \text{and} \ \left.\frac{\partial T_{1_i}}{\partial y}\right|_{bw}. \quad \text{In order to be}$$

able to advance the temperature by one time step at each i these values will be used and assumed constant in the heat balance equation at each time step. For each i the only variable in the corresponding equation in Equation 13 is the temperature T_i.

Since:

$$\frac{2\epsilon_{1_i}\sigma}{\rho_{\text{Si}}C_{p_{\text{Si}}}h_{\text{Si}}} \geq 0 \ \text{let} \ B^4 = \frac{2\epsilon_{1_i}\sigma}{\rho_{\text{Si}}C_{p_{\text{Si}}}h_{\text{Si}}}$$

Since:

$$\frac{1}{2\epsilon_{1_i}\sigma}\left(\epsilon_{1_i}\sum_{j=1}^m F_{1_i 2_j}J_{2_j} + \epsilon_{1_i}G_{lamp} - k_{Ni}\left.\frac{\partial T_{1_i}}{\partial y}\right|_{aw} - k_{Ni}\left.\frac{\partial T_{1_i}}{\partial y}\right|_{bw}\right) \geq 0$$

$$\text{let} \ C^4 = \frac{1}{2\epsilon_{1_i}\sigma}\left(\epsilon_{1_i}\sum_{j=1}^m F_{1_i 2_j}J_{2_j} + \epsilon_{1_i}G_{lamp} - k_{Ni}\left.\frac{\partial T_{1_i}}{\partial y}\right|_{aw} - k_{Ni}\left.\frac{\partial T_{1_i}}{\partial y}\right|_{bw}\right)$$

Rewriting Eq 13 with the substitutions above we arrive at the following ODE:

$$\frac{dT_{1_i}}{dt} = -B^4\left(T_{1_i}^4 - C^4\right) \tag{14}$$

We then massage this equation to obtain a form that allows integration:

$$\frac{dT_{1_i}}{T_{1_i}^2 - C^2} - \frac{dT_{1_i}}{T_{1_i}^2 + C^2} = -2C^2 B^4 dt \tag{15}$$

Integration over the interval $[t, t + \Delta t]$ of this equation leads to the following explicit solution of the above ODE:

$$\frac{1}{2C} \ln \left| \frac{T_{1_i} - C}{T_{1_i} + C} \right|_{t+\Delta t} - \frac{1}{C} \arctan \left(\frac{T_{1_i}}{C} \right)_{t+\Delta t} - \frac{1}{2C} \ln \left| \frac{T_{1_i} - C}{T_{1_i} + C} \right|_t + \frac{1}{C} \arctan \left(\frac{T_{1_i}}{C} \right)_t$$

$$= -2C^2 B^4 \Delta t$$

$$\tag{16}$$

We can now advance the temperature at each A_{1_i} by one time step, using Newton's method described in the following section.

4.4 Applying Newton's method

Since we are advancing the solution by one time step Δt the independent variable is Δt where as t is constant, so that anything evaluated at t is a constant and we are interested in solving the equation for T_{1_i} at $t + \Delta t$. We will apply Newton's method as it proves to be very efficient and accurate applied to this equation, though other numerical methods or solvers can be used in it's place. We will drop the subscript 1_i since the equation is of the exact same form for all i, but remembering that the corresponding equation must be solved at each i on surface A_1 with the corresponding information.

Let $T^* = T(t + \Delta t)$ and $T_o = T(t)$

let $g(T^*) = \dfrac{1}{2C} \ln \left| \dfrac{T^* - C}{T^* + C} \right| - \dfrac{1}{C} \arctan \left(\dfrac{T^*}{C} \right) - \dfrac{1}{2C} \ln \left| \dfrac{T_o - C}{T_o + C} \right| + \dfrac{1}{C} \arctan \left(\dfrac{T_o}{C} \right) +$
$2C^2 B^4 \Delta t$

$$\implies g'(T^*) = \frac{2C^2}{T^{*4} - C^4}$$

Newton's method is given by:

$$T_o^* = T_o$$

$$T_{n+1}^* = T_n^* - \frac{g\left(T_n^*\right)}{g\prime\left(T_n^*\right)} \tag{17}$$

Applying Newton's method to the heat balance equation we arrive at the following recursive algorithm for solving the temperature for the time advance Δt.

$$T_o^* = T\left(t\right)$$

$$T_{n+1}^* = T_n^*$$

$$-\left(\frac{1}{2C}\ln\left|\frac{T_n^* - C}{T_n^* + C}\frac{T_o + C}{T_o - C}\right| - \frac{1}{C}\left(\arctan\left(\frac{T_n^*}{C}\right) - \arctan\left(\frac{T_o}{C}\right)\right) + 2C^2 B^4 \Delta t\right)\frac{T_n^{*^4} - C^4}{2C^2} \tag{18}$$

For this equation and typical RTP variable values we need between 3 to 5 iterations of Newton's method to achieve a solution of the ODE, accurate to within computer roundoff error.

5 Results

In this chapter we discuss the results obtained using a C++ program that follows the model guidelines described in this thesis. The program is designed to numerically solve for temperature along the wafer. The first section defines the parameter inputs used in the numerical experiments produced with the program and the resultant series of graphs produced are found at the end of this chapter. The second section discusses the figures from the first part including: typical temperature profiles as a function of time for the typical RTP process considered for this thesis, difference in temperature between the center and the edge of the wafer through a process run, the drop off of temperature from the center to the edge of the wafer at peak temperatures (where the difference between center and edge is the largest), the effects of varying showerhead diameters and guard ring widths, the effects of varying the showerhead reflectivities and the chamber heights.

5.1 Data and Simulation

For the numerical experiments various input parameters are needed. We are interested in studying the sensitivity of the following parameter inputs: the radius of the showerhead, the width of the guard ring, the reflectivity of the showerhead, and the space between the showerhead and the wafer denoted by chamber height. Unless the variation of these parameters is expressed in the legend, then the input parameters that are used are those defined here.

Power is increased linearly in time from zero to 28.9 W/cm^2 in 5 seconds, the power is then kept at this peak for 40 seconds and then the lamp is turned off.

The reflectivity of the showerhead is 2%.

The gap between the wafer and the guard ring is 0.25mm.

The diameter of the silicon wafer is 200mm.

The emissivity of the silicon wafer is 0.68.

The guard ring width is 25mm.

The showerhead radius is equal to 125.25mm, this equals the outer radius of the guard ring.

The chamber height is 1cm.

The first graph displays the temperature profile at the center of the wafer using Vortek data and the second graph represent our numerical results for comparison. The two input parameters that are significantly different than those defined above are the chamber height and the power input. The chamber

24

height used for these experiments is 5.715mm. In the Vortek experiment the wafer was heated up in 2 seconds to peak power at 420 Amps. Then held for 19 seconds at 420 Amps. Then held at 410 Amps for 11 seconds. This input translates to about 28.9 W/cm^2 corresponding to 420 Amps and 410 Amps is slightly lower at about 27.8 W/cm^2. These numbers were derived by extrapolating from a purely black chamber where peak is 480 Amps, Lefrancois (2001).

5.2 Discussion

Temperature profile: Figure 8 is a graph of the temperature profile at the center of the wafer from the simulation of a process run. This profile is in accordance with typical temperature profiles as those found by Vortek from experimental data from a Sensarray wafer (thermocouple embedded) as shown in Figure 7. There is a difference in the shape of the profile during the heating which may be improved by including a better model of the emissivity for temperatures lower than 700 °C. Further improvements may be possible if a better model for convection is used.

Temperature difference profile: Figure 9 is the profile of the temperature difference between the center of the wafer to the edge through a simulation process run. From this graph we see that the largest differences in temperatures occur between the corner of ramp up and the peak steady state temperature reached by the wafer. As Lefrancois Lefrancois explains, "I would expect greatest temperature difference in most systems is at corner of ramp up - maximum temperature and leveling of profile - it may not be visible at the rates here and because we have a guard ring, but it is observed in many highly reflecting chambers (they have to add power to edge to compensate). Here is why - consider a nonuniformity in heating (and edges usually exhibit this to some extent). During ramp the temperature increases in proportion to the flux ($\rho C_p T$ terms). At temperature - or steady state - the temperature is related to the flux by σT^4. Thus, a variation in flux will be about 4 times smaller at steady state than while ramping. So I expect the worst nonuniformity at the corner as transition between the two types of heating occurs," Lefrancois (2001) Therefore in order to optimize the temperature uniformity along the wafer it will be useful to optimize the temperature uniformity focusing on the profiles at the peak temperatures. The saw-tooth profile that appears in the cooling stage in Figure 9 is not a physical possibility, it is a result of the numerical errors at each time step.

Temperature drop off from wafer center to edge: Figure 10 shows the profile on the wafer starting at the center of the wafer along to the edge. This shows the typical profile of how the temperature varies from the center to the edge of the wafer at the peak temperature, at time t = 40s. The temperature drop off that we see here is because the center of the wafer simply "sees" more of the showerhead and so is exposed to the more of the radiant energy reflected from it. The center will be the hottest point and each point along the wafer will be exposed to less and less radiation as you go out. The closer you are

25

to the center the smaller the drop off and so this reason a guard ring is used around the wafer so that it can take the drop off effects and thus making the wafer more uniform. In the following graphs will plot the temperature drop off at the peak temperatures as it will be useful to show the effects of varying geometries and reflectivities.

Different showerhead diameters: The graph of Figure 11 shows the temperature profiles of varying showerhead diameters, at time t = 40s. When the showerhead diameter is larger than the outer diameter of the guard ring most of the energy is wasted and uniformity improvements are not so noticeable, however uniformity improvements are much more apparent from a smaller showerhead diameter to a diameter that is the same size as the outer diameter of the guard ring. For better uniformity it is important to have the showerhead diameter the same size or larger as the outer diameter of the guard ring.

Different Guard ring widths: Figure 12 shows the temperature profiles of varying guard ring widths, at time t = 40s. From this graph we see that the best uniformity occurs along the wafer when the guard ring width is the largest given financial and mechanical constraints.

Different reflectivities: Figure 13 shows three different temperature profiles corresponding to different showerhead reflectivities (which would correspond to different showerhead materials), at time t = 40s. A perfect black showerhead would have a reflectivity of 0%, however in practice it is only possible to attain a 2% reflective material. It is clear from this graph that the 2% reflective showerhead leads to the most uniform temperature profile and would thus be the best. However as mentioned before there are constraints that would lead a manufacturer to avoid such a low reflective material. For example, if you use the lower reflective material you will need to use more energy from the lamp source in order to achieve the same peak temperature necessary for the process.

Different chamber heights: Figure 14 is a graph that shows the temperature profiles along the wafer for various chamber heights, at time t = 40s. It is clear in the legend that the smaller chamber height minimizes the temperature difference from the center of the wafer to the edge of the wafer.

Figure 7: Vortek data at wafer center
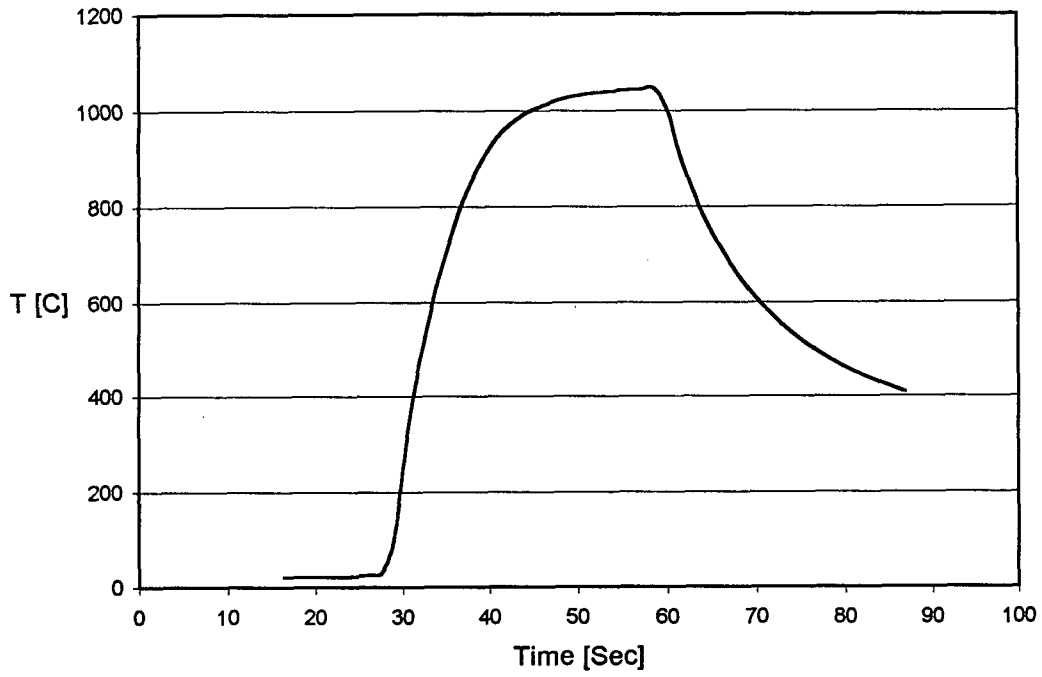
Figure 8: Numerical simulation data at wafer center
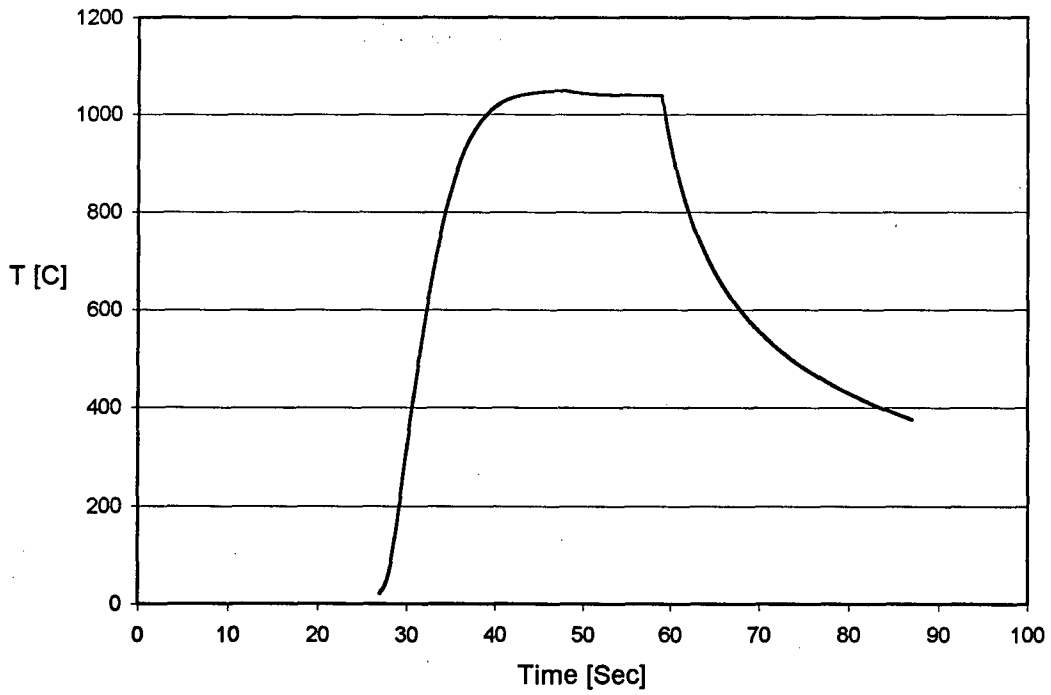
Figure 9: Temperature difference from wafer center to edge
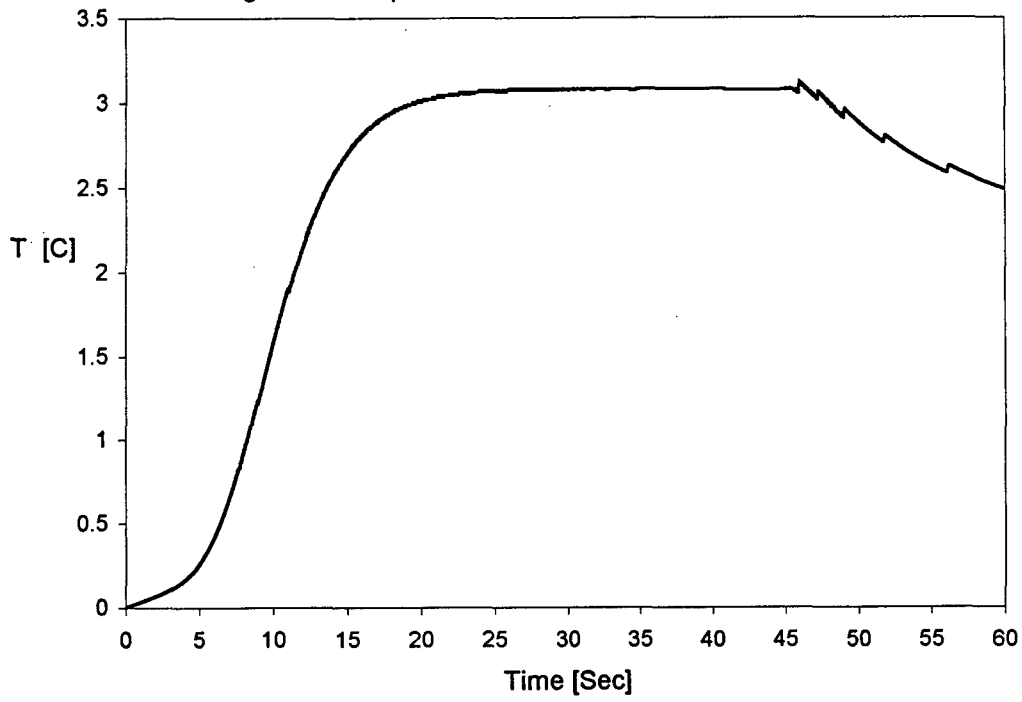
Figure 10: Temperature drop off at time t = 40s

Figure 11: Temperature drop off for different showerhead radii at time t = 40s
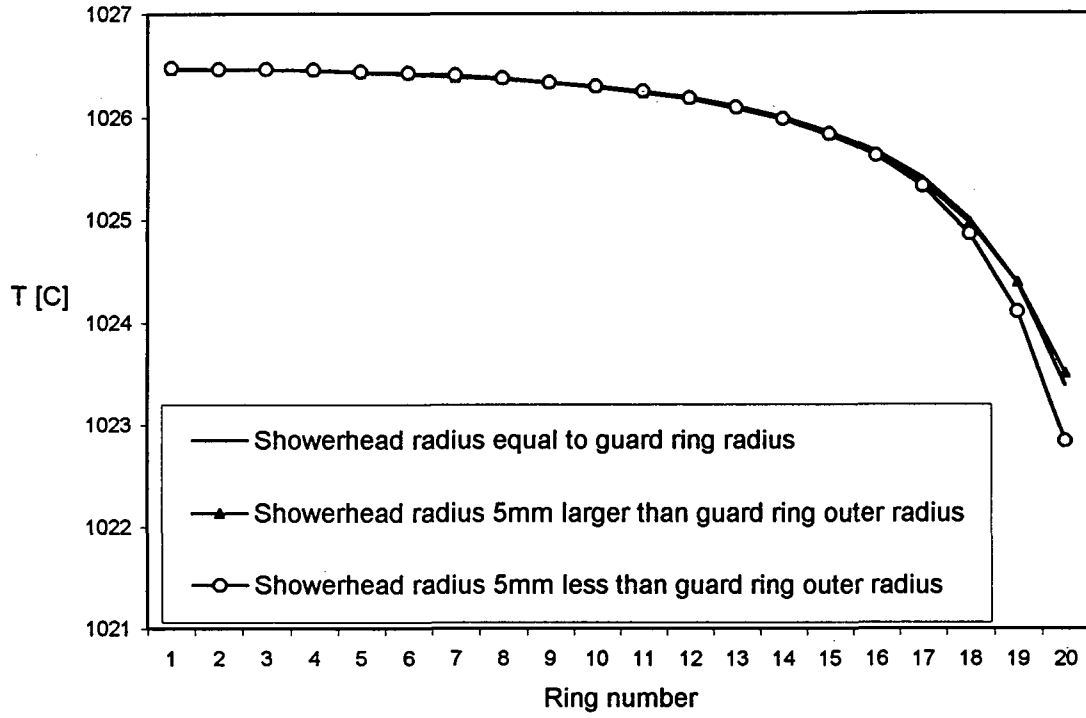
Figure 11: Temperature drop off for different showerhead radii at time t = 40s

Legend:
— Showerhead radius equal to guard ring radius
—▲— Showerhead radius 5mm larger than guard ring outer radius
—○— Showerhead radius 5mm less than guard ring outer radius

T [C] (vertical axis)
Ring number (horizontal axis)

Figure 12: Temperature drop off for different guard ring widths at time t = 40s

Figure 12: Temperature drop off for different guard ring widths at time t = 40s

Legend:
—○— 20mm width guard ring
— 25mm width guard ring
—▲— 30mm width guard ring

T [C] (vertical axis)
Ring number (horizontal axis)
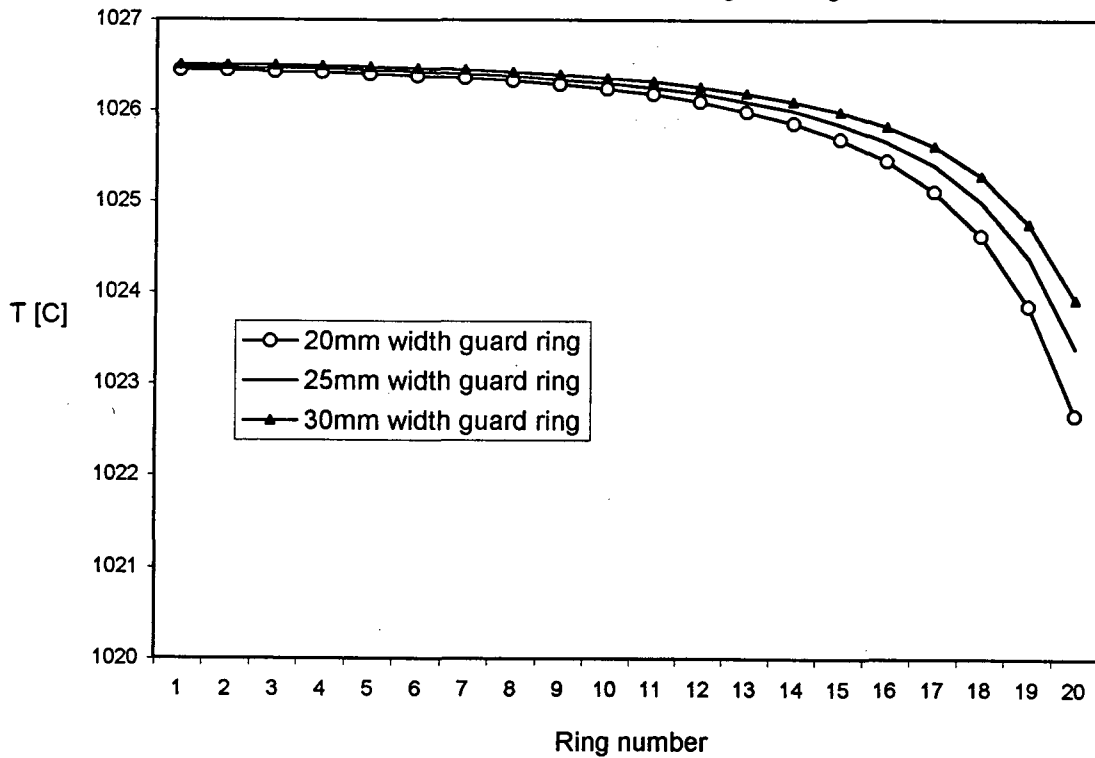
Figure 13: Temperature drop off for different reflectivities at time t = 40s

- 2% reflective showerhead
- 50% reflective showerhead
- 70% reflective showerhead
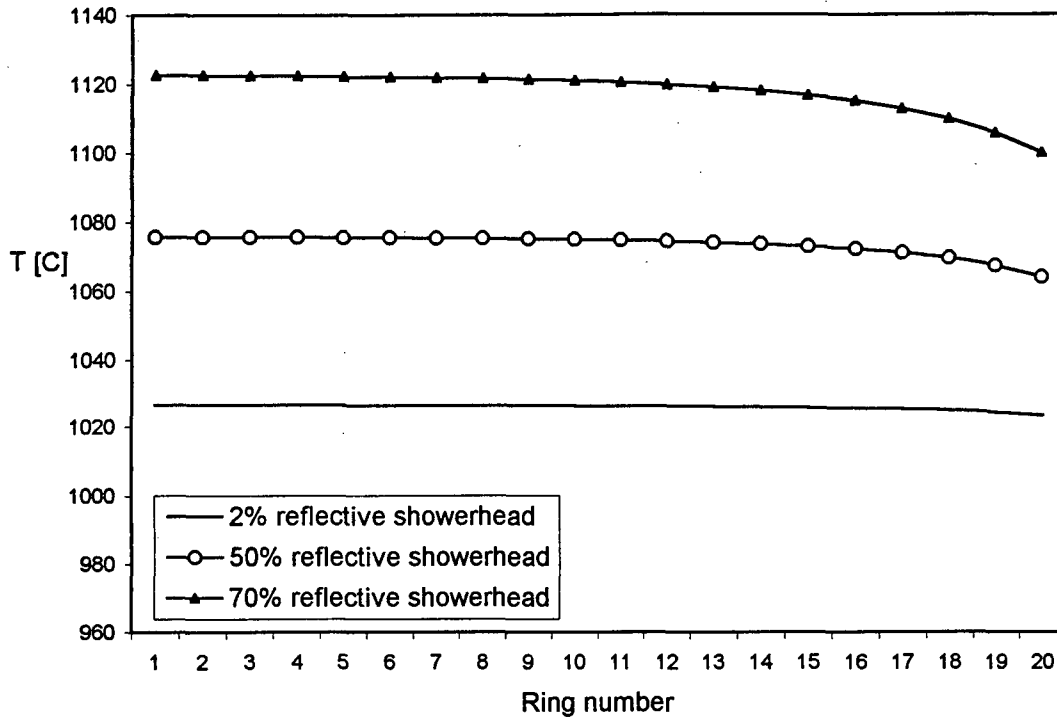
Figure 14: Temperature drop off for different chamber heights at time t = 40s

Chamber height	Temperature difference center-edge
1cm	0.2362%
1.1cm	0.2626%
1.3cm	0.3116%
1.5cm	0.3556%
1.8cm	0.4120%
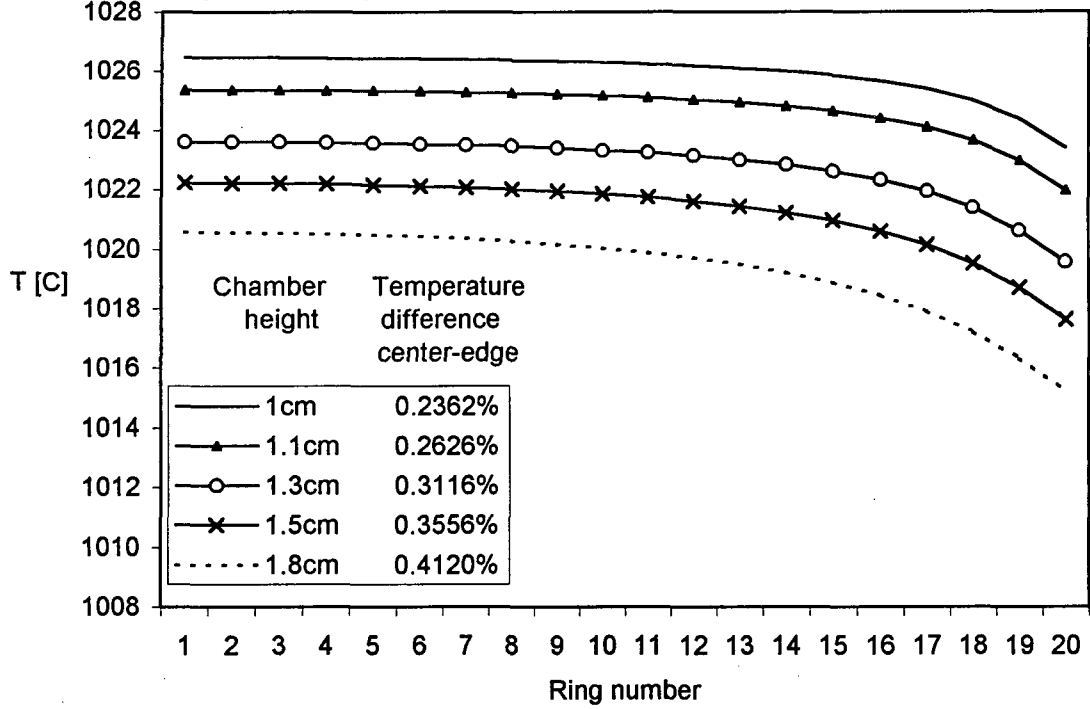
6 Recommendations and Future Work

In the first section of this chapter we make recommendations on how to obtain improved temperature uniformity along the wafer, based on the conclusions made in Chapter Five The second section is an outline of suggested future work in this area in order to improve temperature uniformity results.

6.1 Recommendations

Showerhead size: The showerhead should have the same radius as or a larger radius than the guard ring outer radius to improve the uniformity. For practical purposes however the chamber should be maintained relatively small, less than 300mm in diameter so the radius of the showerhead should be kept below these limits.

Guard ring size: From the graphs it appears that the larger the guard ring the more uniform the temperature will be and so I would recommend using as large a guard ring as possible. For practical purposes the guard ring should be no more than about 1 inch in width since beyond this point too much power is needed to keeping the guard ring hot making it an expensive process.

Reflectivity of the showerhead: From the graph it is clear that the lower the reflectivity the more uniform the temperature will be, however the reflector minimizes the amount of power needed from the lamp to achieve the peak temperatures and so some reflectivity is useful to reduce the amount of power used and in practice any material used will have some reflectivity. I would recommend using a material with as little reflectivity as possible given the constraints on power. "One of the main concerns for the material used for the showerhead is that it be made of a material that does not contaminate the processing chamber in order to process a high value wafer," Lefrancois (2001). For practical purposes of the three reflectivities represented are two that may be used: 1- regular electropolished stainless steel which has 70% reflectivity and is what is currently used in the Vortek chamber and 2- Black anodized or hard anodized steel which have 2% reflectivity.

Chamber height: Once the guard ring width and showerhead material have been established given financial and mechanical constraints, I would recommend to use a chamber height close to 1cm or smaller, ideally the smallest chamber height attains the best temperature uniformity. However in practice there will be a flow included in the RTP process to further improve temperature uniformity and so the flow will need to be considered in conjunction with the knowledge that a smaller gap aids in improved uniformity. If the flow is impinging on the wafer surface, a too small a chamber height will create cool spots as those found by Vortek in experiments where they made the chamber height too small. If however the flow is parallel to the wafer, this would resolve the cold spots and one can take advantage of the improved uniformity resultant of the small chamber height.

Flow profile: Gas flows are typically used in RTP machines to reduce the temperature non-uniformities created by the reflections in the chamber.

Currently the Vortek chamber inserts gas from the showerhead perpendicular to the wafer surface and depending on the distance between the showerhead and the wafer, cold spots or cool patterns appear on the wafer due to the impinging flow. Since it is desirable to take advantage of the uniformity resultant of a small distance between the showerhead and the wafer I would recommend a uniform and axially symmetric profile coming from a thin pipe source connected to the reflecting showerhead, like shown in Figure 15. The flow would be tangential to the wafer and still takes advantage of the uniformity improvement of the reflector and circular wafer but removes the possibility of cold spots when flow is fast enough to make the profile fully developed. Making the flow fully developed removes the possibility of convective cells. The flow will then cool the center of the wafer more than the edges (where it is needed) since the velocity will be higher at the center and will thus take more energy away from the hotter center, aiding in uniformity.

6.2   Future work

- Study the effects of various axially symmetric flow profiles to understand the sensitivity of the shape of the profile to the temperature uniformity. A simple study of this may be done by assuming different flow profiles on a grid or mesh that covers the chamber domain around the wafer. One can then solve the energy equation substituting in the flow velocities and using a simple algorithm like Point Gauss Seidel to obtain a temperature profile in the chamber. A program like the one in this thesis should be used as a boundary condition on the wafer.

- Study the effects of the flow profiles currently attainable in the Vortek RTP chamber. This study may be done using a model like that in Appendix C which would need to be solved using a commercial software package or with a CFD program to implement the equations in the appendix.

- Study the effects of possible convective cells. The hot wafer causes convection of the gas between it and the cold walls, which influence the flow patterns and temperature uniformity. Thus in order to design a successful RTP device it is important to understand the details of the gas flow and its influence on temperature uniformity. A three dimensional Computational Fluid Dynamics (CFD) model should be developed for predicting the gas flows and temperature profiles inside the RTP chamber. The model in Appendix C is intended to study the effects of the fluid dynamics, however since a main assumption of the model is that the problem is axially symmetric, it is important to note that in order to study the effects of convective cells that may occur in the chamber a full three dimensional model would need to be solved. A program like the one in this thesis could be used as a boundary condition on the wafer to solve the fluid problem.

View from the side

reflecting surface

wafer

View from above
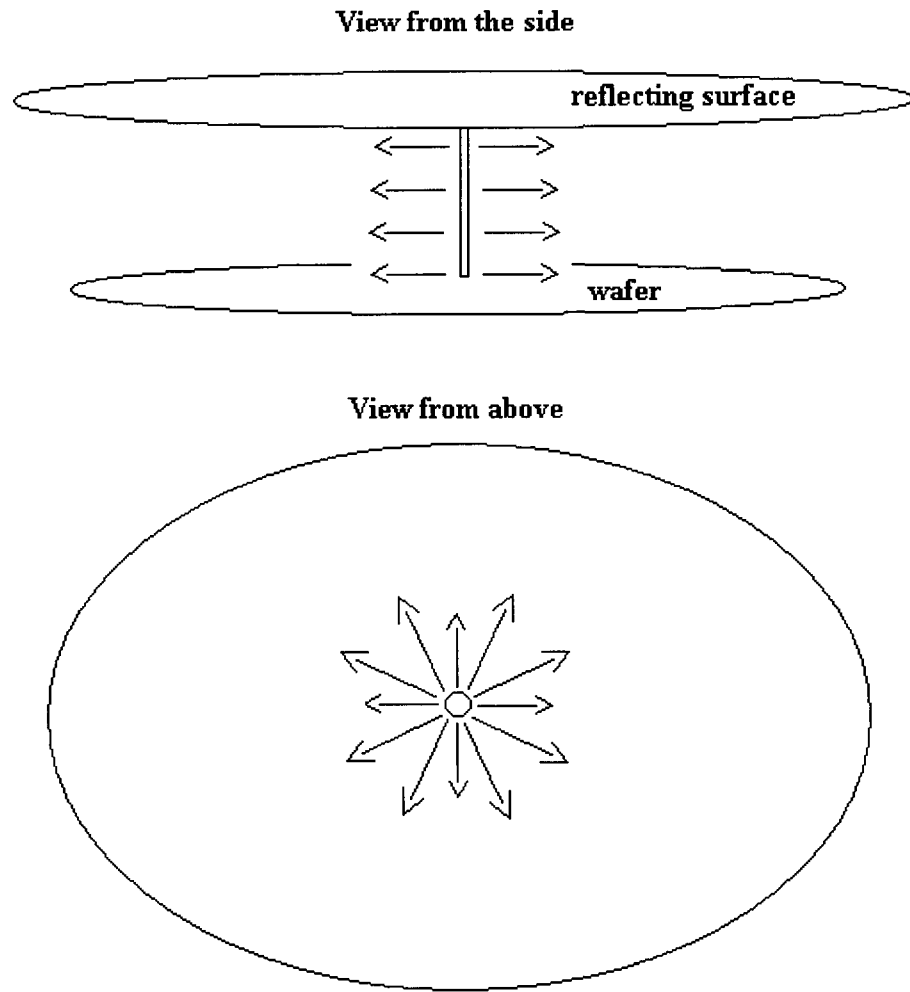
Figure 15: Uniform axially symmetric flow profile

References

[1] Anderson, Dale A. et al. (1984) "Computational Fluid Mechanics and Heat Transfer," Hemisphere Publishing Corporation, New York. A subsidiary of Harper & Row, Publishers, Inc. pp. 181-197

[2] Batchelor, G.K. (1967) "An Introduction to Fluid Dynamics," Cambridge University Press

[3] Brady, George S. (1972) "Materials Handbook," New York: McGraw-Hill, 10th edition, Vol 2.

[4] Camm, David M. (1996) "Rapid Thermal Processing Apparatus and Method", patent number: 5,561,735, United States Patent

[5] Chapman, A.J. (1967) "Heat Transfer," The Macmillan Company, New York/Collier-Macmillan Limited, London. pp. 392-441

[6] Hiester, N.K. et al (1957) "A solar furnace with parabolic aluminum reflector", Journal of the American Rocket Society, Vol. 27, pp 507

[7] Hirschfelder, J.O. et al (1954). "Molecular Theory of Gases and Liquids," Wiley, New York

[8] Kreith, F. (1962) "Radiation Heat Transfer for Spacecraft and Solar Power Plant Design," International Textbook Company, Scranton, Pennsylvania

[9] Lefrancois, Marcel. Personal Communication, 2001.

[10] Lide, David R. (1993) "CRC Handbook of Chemistry and Physics," 73rd Edition, Special student edition, CRC Press, p 6-19

[11] Lojek, B. (1999) "Early History of Rapid Thermal Processing," RTP'99, 7th International Conference on Advanced Thermal Processing of Semiconductors, p. 292-317

[12] Press, William H. et al. (1992) "Numerical Recipies in C: The Art of Scientific Computing" Second Edition, Cambridge University Press. pp. 46-47

[13] Reid, R.C. et al. (1977). "The Properties of Gases and Liquids," 3rd ed., McGraw-Hill, New York

[14] Rozemboom F. (1996) "Advances in Rapid Thermal and Integrated Processing," Kluwer Academic Publishers. pp. 265-304

[15] Sato, Tsutomu. (1967) "Spectral emissivity of Silicon," Japenese Journal of Appled Physics. Vol. 6, No. 3, p. 339

[16] Schlichting, H. (1968) "Boundary-Layer Theory," 6th ed., translated by J. Kestin, McGraw-Hill, New York

[17] White, Frank. M. (1974). "Viscous Fluid Flow," McGraw-Hill, New York

[18] White, Frank M. (1986). "Fluid Mechanics," McGraw-Hill, Inc. pp. 245-280
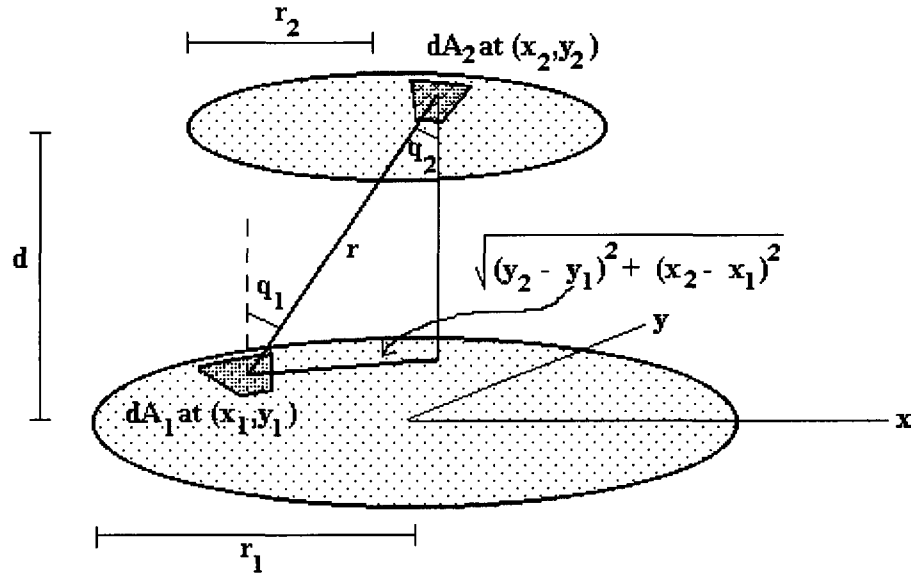
Figure 16: Geometry between two disks

A Evaluation of the Shape Factor

The purpose of this appendix is to define a numeric formula for calculating the fraction of radiant energy leaving a ring shaped surface A_1 that is incident on a parallel ring shaped surface A_2. The material in this appendix has been extracted from: Krieth (1962) and Chapman (1967). This appendix begins with the definition of shape factor and states the basic reciprocity law and the decomposition law which are necessary to do shape factor manipulation. First we split up two parallel disks each into a ring and a disk. We do some shape factor manipulations to achieve a shape factor relation from the ring of one surface to the disk of the other. We continue to derive the shape factor relation for a ring to the other ring. Finally we express the shape factor for a disk of radius r_1 to a disk of radius r_2 dependent only on the two radii and the distance that separates them. In addition the ring to disk and ring to ring shape factors derived are expressed so that they depend only on the disk to disk calculation so that no further calculations are required.

Definition 1 *Shape-Factor*

  The Shape or configuration factor from A_1 to A_2, written F_{12}, may be defined

35
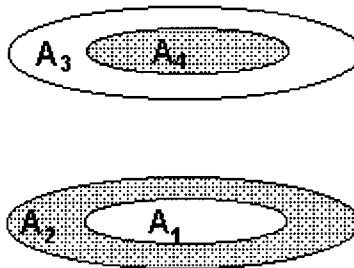
Figure 17: Division of areas into rings and disks

as the fraction of the total radiant energy leaving A_1 that is incident upon A_2. The shape factor is a function of the geometry of the two surfaces A_1 and A_2 and depends also on the directional distribution of the radiation from the source. For the purpose of this thesis the directional distribution of the radiant emission has been assumed to follow Lambert's cosine law, so that

$$F_{12} = \frac{1}{A_1} \int_{A_1} \int_{A_2} \frac{\cos(q_1)\cos(q_2)}{\pi r^2} dA_2 dA_1 \tag{19}$$

This method makes use of various principles, two of which will be summarized here.

Basic Reciprocity Law. The product of an Area A_1 and the shape factor of A_1 relative to another area A_2, i.e., F_{12}, is related to the product of A_2 and F_{21} by the relation

$$A_1 F_{12} = A_2 F_{21} \tag{20}$$

Decomposition Law. Given two surfaces A_a and A_b, if surface A_a is subdivided into A_3 and A_4, then the total shape factor F_{ab} is related to the two subsidiary shape factors F_{3b} and F_{4b} according to

$$A_a F_{ab} = A_3 F_{3b} + A_4 F_{4b} \tag{21}$$

Using the above to derive F_{24} as in Figure 17, the shape factor from the ring A_2 to the disk A_4.

$(A_1 + A_2)F_{(12)4} = A_1 F_{14} + A_2 F_{24}$, this gives the relation

$$F_{24} = \frac{A_1 + A_2}{A_2} F_{(12)4} - \frac{A_1}{A_2} F_{14} \tag{22}$$

36

Similarly we get the relation from a ring A_2 to a ring A_3, F_{23}

$$F_{23} = F_{2(34)} - F_{24} = F_{2(34)} - [\frac{A_1 + A_2}{A_2} F_{(12)4} - \frac{A_1}{A_2} F_{14}] \qquad (23)$$

Using the previous result for ring to disk we may replace $F_{2(34)}$ and arrive at the desired result for F_{23} written in the following form that only involves disk to disk shape factors.

$$F_{23} = \frac{1}{A_2}\{(A_1 + A_2)[F_{(12)(34)} - F_{(12)4}] - A_1[F_{1(34)} - F_{14}]\} \qquad (24)$$

Since all the shape factors may be written in terms of disk to disk shape factors as shown above we only need a formula for calculating the shape factor from a disk to a disk. Derivation of the shape factor for a disk of radius r_1 to a disk of radius r_2 using the definition of shape factor and referring to Figure 16: Let

$$x_1 = \widehat{r_1}\cos(\widehat{\phi_1}), \ y_1 = \widehat{r_1}\sin(\widehat{\phi_1}) \qquad 0 \le \widehat{r_1} \le r_1, \qquad 0 \le \widehat{\phi_1} \le 2\pi$$

$$x_2 = \widehat{r_2}\cos(\widehat{\phi_2}), \ y_2 = \widehat{r_2}\sin(\widehat{\phi_2}) \qquad 0 \le \widehat{r_2} \le r_2, \qquad 0 \le \widehat{\phi_2} \le 2\pi$$

$$r^2 = d^2 + (y_2 - y_1)^2 + (x_2 - x_1)^2 = d^2 + \widehat{r_1}^2 + \widehat{r_2}^2 - 2\widehat{r_1}\widehat{r_2}\cos(\widehat{\phi_2} - \widehat{\phi_1})$$

$$dA_1 = \widehat{r_1}\,d\widehat{\phi_1}\,d\widehat{r_1}$$

$$dA_2 = \widehat{r_2}\,d\widehat{\phi_2}\,d\widehat{r_2}$$

$$F_{12} = \frac{1}{\pi r_1^2} \int_0^{2\pi} \int_0^{r_2} \int_0^{2\pi} \int_0^{r_1} \frac{\cos(q_1)\cos(q_2)}{\pi r^2} \widehat{r_1}\widehat{r_2}\,d\widehat{r_1}\,d\widehat{\phi_1}\,d\widehat{r_2}\,d\widehat{\phi_2} \qquad (25)$$

$$\cos(q_1) = \cos(q_2) = \frac{d}{r} = \frac{d}{\sqrt{d^2 + \widehat{r_1}^2 + \widehat{r_2}^2 - 2\widehat{r_1}\widehat{r_2}\cos(\widehat{\phi_2} - \widehat{\phi_1})}} \qquad (26)$$

$$F_{12} = \frac{1}{\pi r_1^2} \int_0^{2\pi} \int_0^{r_2} \int_0^{2\pi} \int_0^{r_1} \frac{d^2\,\widehat{r_1}\,\widehat{r_2}}{\pi(d^2 + \widehat{r_1}^2 + \widehat{r_2}^2 - 2\widehat{r_1}\,\widehat{r_2}\cos(\widehat{\phi_2} - \widehat{\phi_1}))^2} d\widehat{r_1}\,d\widehat{\phi_1}\,d\widehat{r_2}\,d\widehat{\phi_2} \qquad (27)$$

$$F_{12} = \frac{1}{2}(x - \sqrt{x^2 - 4E^2 D^2}) \qquad (28)$$

where: $E = \dfrac{r_2}{d}, D = \dfrac{d}{r_1}$ and $x = 1 + (1 + E^2)D^2$

B Solving the heat exchange system of equations.

The purpose of this appendix is to explain how the system of equations derived from the heat exchange between the wafer surface and the showerhead surface is solved to obtain the total irradiation at the surface of the wafer. This appendix begins by expanding the system of equations relating irradiation to temperature as described in chapter four. The system is then written in matrix form and with matrix manipulation it is written as a simplified matrix equation. The system is ready to solve in its simplified form using LU decomposition with pivoting. However, this is an $(m+n)$ by $(m+n)$ system of equations which can be relatively large. We take advantage of the form of the simplified system to reduce it to a system of m by m equations, which can be solved more quickly.

From chapter 4 the system of equations is given by:

$$J_{1_i} = \epsilon_{1_i}\sigma T_{1_i}^4 + (1 - \epsilon_{1_i})\sum_{j=1}^m F_{1_i 2_j} J_{2_j} \quad for \; i = 1..n.$$

$$J_{2_j} = \epsilon_{2_j}\sigma T_{2_j}^4 + (1 - \epsilon_{2_j})\sum_{i=1}^n F_{2_j 1_i} J_{1_i} \quad for \; j = 1..m.$$

(29)

Rewriting this in the expanded form:

$$J_{1_i} = \epsilon_{1_1}\sigma T_{1_1}^4 + (1 - \epsilon_{1_1})(F_{1_1 2_1} J_{2_1} + F_{1_1 2_2} J_{2_2} + F_{1_1 2_3} J_{2_3} ... + F_{1_1 2_m} J_{2_m})$$

$$J_{1_2} = \epsilon_{1_2}\sigma T_{1_2}^4 + (1 - \epsilon_{1_2})(F_{1_2 2_1} J_{2_1} + F_{1_2 2_2} J_{2_2} + F_{1_2 2_3} J_{2_3} ... + F_{1_2 2_m} J_{2_m})$$

$$J_{1_3} = \epsilon_{1_3}\sigma T_{1_3}^4 + (1 - \epsilon_{1_3})(F_{1_3 2_1} J_{2_1} + F_{1_3 2_2} J_{2_2} + F_{1_3 2_3} J_{2_3} ... + F_{1_3 2_m} J_{2_m})$$

...

$$J_{1_n} = \epsilon_{1_n}\sigma T_{1_n}^4 + (1 - \epsilon_{1_n})(F_{1_n 2_1} J_{2_1} + F_{1_n 2_2} J_{2_2} + F_{1_n 2_3} J_{2_3} ... + F_{1_n 2_m} J_{2_m})$$

$$J_{2_1} = \epsilon_{2_1}\sigma T_{2_1}^4 + (1 - \epsilon_{2_1})(F_{2_1 1_1} J_{1_1} + F_{2_1 1_2} J_{1_2} + F_{2_1 1_3} J_{1_3} .... + F_{2_1 1_n} J_{1_n})$$

$$J_{2_2} = \epsilon_{2_2}\sigma T_{2_2}^4 + (1 - \epsilon_{2_2})(F_{2_2 1_1} J_{1_1} + F_{2_2 1_2} J_{1_2} + F_{2_2 1_3} J_{1_3} ... + F_{2_2 1_n} J_{1_n})$$

...

$$J_{2_m} = \epsilon_{2_m}\sigma T_{2_m}^4 + (1 - \epsilon_{2_m})(F_{2_m 1_1} J_{1_1} + F_{2_m 1_2} J_{1_2} + F_{2_m 1_3} J_{1_3} ... + F_{2_m 1_n} J_{1_n})$$

The above system written in matrix form is:

$$IJ = T + FJ$$

(30)

In the above matrix equation, I is the identity matrix with $(n + m)$ rows and $(n + m)$ columns (0's everywhere except on the diagonal). T is a vector

dependent on temperature: the first n elements have as an ith entry: $\epsilon_{1_i}\sigma T_{1_i}^4$ and from n to $(n+m)$ the ith entry is: $\epsilon_{2_{i-n}}\sigma T_{2_{i-n}}^4$. J is the irradiation vector which we are wanting to solve for: The first n elements have as an ith entry: J_{1_i} and from n to $(n+m)$ it is: $J_{2_{i-n}}$

$$F = \left[\begin{array}{cc} 0 & F_1 \\ F_2 & 0 \end{array} \right]$$

where F_1 has m columns and n rows and F_2 has n columns and m rows.

$$F_1 = \left[\begin{array}{ccccc} (1-\epsilon_{1_1})F_{1_1 2_1} & (1-\epsilon_{1_1})F_{1_1 2_2} & (1-\epsilon_{1_1})F_{1_1 2_3} & ... & (1-\epsilon_{1_1})F_{1_1 2_m} \\ (1-\epsilon_{1_2})F_{1_2 2_1} & (1-\epsilon_{1_2})F_{1_2 2_2} & (1-\epsilon_{1_2})F_{1_2 2_3} & ... & (1-\epsilon_{1_2})F_{1_2 2_m} \\ (1-\epsilon_{1_3})F_{1_3 2_1} & (1-\epsilon_{1_3})F_{1_3 2_2} & (1-\epsilon_{1_3})F_{1_3 2_3} & ... & (1-\epsilon_{1_3})F_{1_3 2_m} \\ ... & ... & ... & ... & ... \\ (1-\epsilon_{1_n})F_{1_n 2_1} & (1-\epsilon_{1_n})F_{1_n 2_2} & (1-\epsilon_{1_n})F_{1_n 2_3} & ... & (1-\epsilon_{1_n})F_{1_n 2_m} \end{array} \right]$$

$$F_2 = \left[\begin{array}{ccccc} (1-\epsilon_{2_1})F_{2_1 1_1} & (1-\epsilon_{2_1})F_{2_1 1_2} & (1-\epsilon_{2_1})F_{2_1 1_3} & ... & (1-\epsilon_{2_1})F_{2_1 1_n} \\ (1-\epsilon_{2_1})F_{2_2 1_1} & (1-\epsilon_{2_1})F_{2_2 1_2} & (1-\epsilon_{2_1})F_{2_2 1_3} & ... & (1-\epsilon_{2_1})F_{2_2 1_n} \\ ... & ... & ... & ... & ... \\ (1-\epsilon_{2_m})F_{2_m 1_1} & (1-\epsilon_{2_m})F_{2_m 1_2} & (1-\epsilon_{2_m})F_{2_m 1_3} & ... & (1-\epsilon_{2_m})F_{2_m 1_n} \end{array} \right]$$

With some simple matrix manipulation on Equation 30 we arrive at the simplified matrix form:

$$\widetilde{F}J = T \tag{31}$$

$$\widetilde{F} = \left[\begin{array}{cc} I_n & \widetilde{F_1} \\ \widetilde{F_2} & I_m \end{array} \right]$$

$\widetilde{F_1}$ has m columns and n rows, $\widetilde{F_2}$ has n columns and m rows, I_n is the n by n identity matrix and I_m is the m by m identity matrix. $\widetilde{F_1}$ and $\widetilde{F_2}$ are given by:

$$\widetilde{F_1} = \left[\begin{array}{ccccc} -(1-\epsilon_{1_1})F_{1_1 2_1} & -(1-\epsilon_{1_1})F_{1_1 2_2} & -(1-\epsilon_{1_1})F_{1_1 2_3} & ... & -(1-\epsilon_{1_1})F_{1_1 2_m} \\ -(1-\epsilon_{1_2})F_{1_2 2_1} & -(1-\epsilon_{1_2})F_{1_2 2_2} & -(1-\epsilon_{1_2})F_{1_2 2_3} & ... & -(1-\epsilon_{1_2})F_{1_2 2_m} \\ -(1-\epsilon_{1_3}F_{1_3 2_1} & -(1-\epsilon_{1_3})F_{1_3 2_2} & -(1-\epsilon_{1_3})F_{1_3 2_3} & ... & -(1-\epsilon_{1_3})F_{1_3 2_m} \\ ... & ... & ... & ... & ... \\ -(1-\epsilon_{1_n})F_{1_n 2_1} & -(1-\epsilon_{1_n})F_{1_n 2_2} & -(1-\epsilon_{1_n})F_{1_n 2_3} & ... & -(1-\epsilon_{1_n})F_{1_n 2_m} \end{array} \right]$$

$$\widetilde{F_2} = \begin{bmatrix} -(1-\epsilon_{2_1})F_{2_1 1_1} & -(1-\epsilon_{2_1})F_{2_2 1_2} & -(1-\epsilon_{2_1})F_{2_2 1_3} & \dots & -(1-\epsilon_{2_1})F_{2_2 1_n} \\ -(1-\epsilon_{2_1})F_{2_2 1_1} & -(1-\epsilon_{2_1})F_{2_2 1_2} & -(1-\epsilon_{2_1})F_{2_2 1_3} & \dots & -(1-\epsilon_{2_1})F_{2_2 1_n} \\ \dots & \dots & \dots & \dots & \dots \\ -(1-\epsilon_{2_m})F_{2_m 1_1} & -(1-\epsilon_{2_m})F_{2_m 1_2} & -(1-\epsilon_{2_m})F_{2_m 1_3} & \dots & -(1-\epsilon_{2_m})F_{2_m 1_n} \end{bmatrix}$$

The matrix system given in Equation 31 is a simple $(n+m)$ system where the matrix $\widetilde{F}$ has $(n+m)$ rows and $(n+m)$ columns and whose entries are constant. We are interested in solving for the (irradiation) vector J with $(n+m)$ entries. The system will be solved using LU decomposition with pivoting, however we will take advantage of the form of the matrix and reduce the size of the system before solving it.

Given the system from Equation 31:

$$\begin{bmatrix} I_n & \widetilde{F_1} \\ \widetilde{F_2} & I_m \end{bmatrix} \begin{bmatrix} J_1 \\ J_2 \end{bmatrix} = \begin{bmatrix} T_1 \\ T_2 \end{bmatrix}$$

The above system is equivalent to:

$$J_1 + \widetilde{F_1}J_2 = T_1 \quad \implies \quad J_1 = T_1 - \widetilde{F_1}J_2$$

$$\widetilde{F_2}J_1 + J_2 = T_2 \quad \implies \quad \widetilde{F_2}(T_1 - \widetilde{F_1}J_2) + J_2 = T_2$$

$$\implies \quad (I - \widetilde{F_2}\widetilde{F_1})J_2 = T_2 - \widetilde{F_2}T_1$$

$(I - \widetilde{F_2}\widetilde{F_1})$ is called the Schur complement, and for this system it is easy to compute. This system has now been reduced to an m by m system of equations since $(I - \widetilde{F_2}\widetilde{F_1})$ is an m by m matrix and we are solving for the elements of J_2 which has m unknowns. Since m and n are of similar size for the application in this thesis I have chosen to eliminate J_1 first to get an equation for J_2, however you could also eliminate J_2 first and get a similar equation for J_1 of order n rather than m, for example if $n << m$ it would be better to do the latter. Now we can apply LU decomposition with partial pivoting to this reduced system to solve for J_2 and then substitute to get J_1. The algorithm used to solve the system of equations with LU decomposition with Partial Pivoting is called "Crout's algorithm", Press et al. (1992).

C Fluid Model

This appendix outlines a model of the fluid dynamics for an axially symmetric RTP system. The model consists of deriving the full set of equations that describe the relevant physics that take place inside of the chamber during a process run with the corresponding boundary conditions for the specific geometry of an axially symmetric RTP chamber like that of Vortek Industries Ltd. One of the boundaries considered is the boundary which represents the wafer surface; the derivation of the condition at this boundary explains how the radiation model is coupled to the fluid model of this appendix via the radiation boundary condition.

Some physical assumptions and geometry simplifications that are made for this model are described in the first section. In the second section we define the fundamental equations of fluid dynamics and the equations of state for the perfect gas considered in this model. Since the domain considered is axially symmetric, the equations are defined in a cylindrical coordinate system in order to take advantage of the simplifications resultant of the axially symmetric assumption. The third section is dedicated to the non-dimensionalization of the axially symmetric equations. First the non-dimensional variables and parameters that arise in the procedure of non-dimensionalization are defined. After these are defined, all the equations are restated in the final non-dimensional form. Finally in this section we explain how the variation of viscosity and conductivity are included in the non-dimensional equations. In the fourth section we discuss the non-dimensional parameters characteristic of these equations. The final section is the derivation of the boundary conditions that correspond with this fluid model, in which is included a description of how the radiation can be applied as a boundary condition to couple the radiation and fluid models.

C.1 Physical assumptions

Some physical assumptions and geometry simplifications must be made to make this study possible. Once these assumptions have been made one can define a computational domain where the equations of motion described in this appendix can be solved. The following is a description of the simplified computational domain shown below.

The light intensity from the lamp is assumed to be uniform and perpendicular to the wafer lower surface. The silicon wafer will be assumed infinitely thin in the sense that the temperature on the top surface of the wafer will be assumed identical to the temperature on the lower surface. The chamber has an axially symmetric geometry with the exception of the inflow holes in the shower head. By replacing the series of holes with a continuous gap for the inflow at the shower head, the entire geometry may be assumed axially symmetric. An approximation based on convection is used for the temperature gradient below the lower surface of the wafer, which eliminates the lower black chamber from the computational domain. The cooled walls and the showerhead are assigned a fixed temperature boundary condition. The inflow will have an assumed fully

41

Figure 18: Computational domain
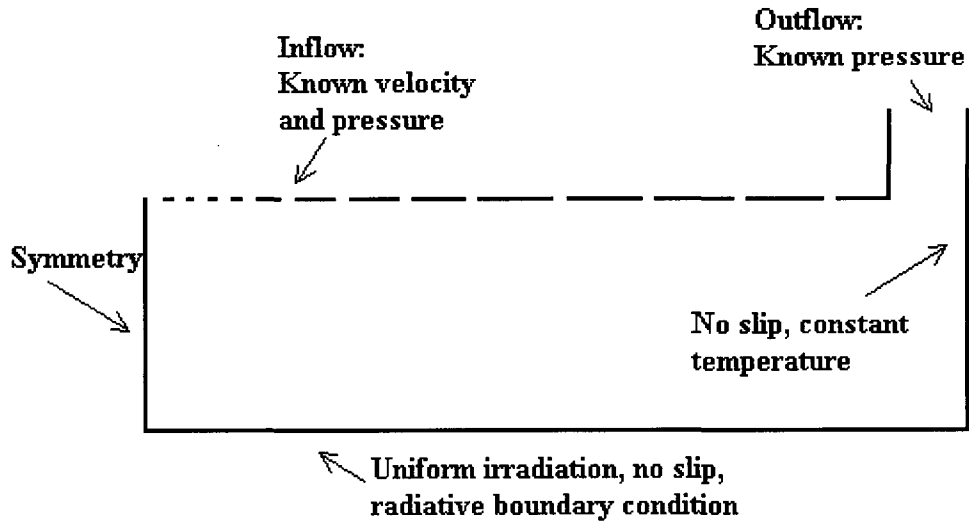
developed flow profile and assumed to be at a fixed temperature. The outflow
will also be assumed to be fully developed and assigned an outflow pressure of
atmospheric pressure. Due to a low Reynolds number typical of RTP systems
the flow will be assumed laminar and continuous.

C.2   Axially symmetric equations of fluid dynamics

The fundamental equations of fluid dynamics are based on Conservation of
Mass, Conservation of Momentum and Conservation of Energy. The equation
resulting from the law of conservation of mass is called the continuity equation.
When the conservation of momentum law, Newton's Second Law, is applied
to fluid flow the resulting equation is called the momentum equation. The
third equation, derived from the First Law of Thermodynamics, is known as
the energy equation. The derivation of the fundamental equations of fluid
dynamics will not be included in this thesis. However, the reader may refer
to the derivation of the equations using the phenomenological approach treated
by Schlichting (1968) and the kinetic approach described by Hirschfelder et
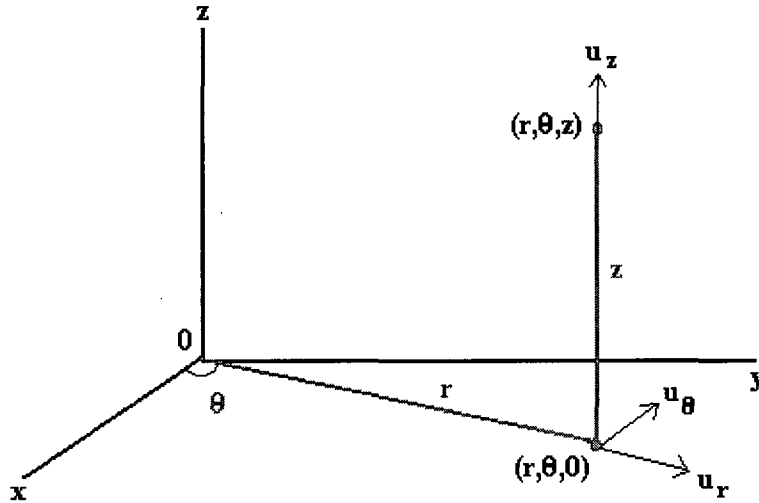
Figure 19:

al.(1954). The fundamental equations given here are derived for a uniform, homogeneous fluid without mass diffusion or finite rate chemical reactions.

The basic equations of fluid dynamics are independent of the coordinate system in which they are expressed. For the purpose of this thesis it is convenient to express these equations using a cylindrical coordinate system. The derivation of these equations in generalized orthogonal curvilinear coordinates is done by Anderson et al (1984).

Defining a three dimensional coordinate system x_1, x_2, x_3 whose origin is fixed:

$x_1 = r$ where r defines the radial location relative to the origin.

$u_1 = u_r$ where u_r is the velocity in the radial direction.

$x_2 = \theta$ where θ defines the angular location.

$u_2 = u_\theta$ where u_θ is the angular velocity.

$x_3 = z$ where z defines the distance perpendicular to the $r - \theta$ plane.

$u_3 = u_z$ where u_z is the velocity in the z direction.

For an axisymmetric compressible flow (all variables are independent of θ), with gravity acting in the -z direction, without heat sources, the equations of fluid dynamics using the above coordinate system are given by:

C.2.1 Continuity equation

$$\frac{\partial (\rho r)}{\partial t} + \frac{\partial (\rho r u_r)}{\partial r} + \frac{\partial (\rho r u_z)}{\partial z} = 0 \qquad (32)$$

43

where ρ is the fluid density

C.2.2 r-Momentum equation

$$\frac{\partial (\rho r u_r)}{\partial t} + \frac{\partial}{\partial r} \left(\rho r u_r^2 - r\Pi_{rr} \right) + \frac{\partial}{\partial z} \left(\rho r u_r u_z - r\Pi_{rz} \right) =$$

$$P - \frac{2}{3}\mu \left(2\frac{u_r}{r} - \frac{\partial u_r}{\partial r} - \frac{\partial u_z}{\partial z} \right) \tag{33}$$

where μ is the coefficient of dynamic viscosity and

$$\Pi_{rr} = \left(-P + \frac{2}{3}\mu \left(2\frac{\partial u_r}{\partial r} - \frac{u_r}{r} - \frac{\partial u_z}{\partial z} \right) \right) \tag{34}$$

$$\Pi_{rz} = \mu \left(\frac{\partial u_r}{\partial z} + \frac{\partial u_z}{\partial r} \right) \tag{35}$$

C.2.3 z-Momentum equation

$$\frac{\partial (\rho r u_z)}{\partial t} + \frac{\partial}{\partial r} \left(\rho r u_r u_z - r\Pi_{rz} \right) + \frac{\partial}{\partial z} \left(\rho r u_z^2 - r\Pi_{zz} \right) = -\rho r g \tag{36}$$

where $g = 9.807 m/s^2$ is the body force given by the acceleration of gravity and

$$\Pi_{zz} = \left(-P + \frac{2}{3}\mu \left(2\frac{\partial u_z}{\partial z} - \frac{\partial u_r}{\partial r} - \frac{u_r}{r} \right) \right) \tag{37}$$

C.2.4 Energy equation

$$\frac{\partial (rE_t)}{\partial t} + \frac{\partial (rE_t u_r)}{\partial r} + \frac{\partial (rE_t u_z)}{\partial z} = \left(\frac{\partial}{\partial r} \left(kr\frac{\partial T}{\partial r} \right) + \frac{\partial}{\partial z} \left(kr\frac{\partial T}{\partial z} \right) \right) - \rho g r u_z +$$

$$\frac{\partial}{\partial r} \left(r \left(\Pi_{rr} u_r + \Pi_{rz} u_z \right) \right) + \frac{\partial}{\partial z} \left(r \left(\Pi_{rz} u_r + \Pi_{zz} u_z \right) \right) \tag{38}$$

where E_t is the total energy per unit volume given by:

$$E_t = \rho \left(e + \frac{U^2}{2} + \text{potential energy} \right) \tag{39}$$

where e is the internal energy per unit mass.

44

C.2.5 Equation of state

According to the State Principle of thermodynamics, the local thermodynamic state is fixed by any two independent thermodynamic variables provided that the chemical composition of the fluid is not changing due to diffusion or finite-rate chemical reactions. For a perfect gas, the equations of state are:

$$P = \rho R T \tag{40}$$

$$e = c_v T \tag{41}$$

where R is the gas constant. Also, correspondingly the following relations exist:

$$\gamma = \frac{c_p}{c_v} \qquad c_v = \frac{R}{\gamma - 1} \qquad c_p = \frac{\gamma R}{\gamma - 1} \tag{42}$$

where c_v is the specific heat at constant volume, c_p is the specific heat at constant pressure and γ is the ratio of the specific heats. For further details on the derivations above refer to Anderson et al (1984). Using these relations we can express P and T as functions of ρ and e:

$$P = (\gamma - 1)\rho e \qquad T = \frac{(\gamma - 1)e}{R} \tag{43}$$

C.3 Non-dimensionalization of equations

In this section the governing equations will be put into nondimensional form. Nondimensionalization expresses characteristic parameters such as Reynolds number, Prandtl number, etc., (explained in more detail in the following section), and makes it easy to vary physical parameters of a problem, such as different gases, flow velocities, etc. Another advantage of the nondimensionalized equations is that the flow variables are normalized so that their values are typically of order 1, many times making it easier to analyze the results.

Define L as the reference length and use "ref" as the subscript for the reference values. For example V_{ref} is the reference velocity. The non-dimensional variables can then be written as

$$r^* = \frac{r}{L} \qquad z^* = \frac{z}{L} \qquad u_r^* = \frac{u_r}{V_{ref}} \qquad u_z^* = \frac{u_z}{V_{ref}}$$

$$t^* = \frac{t}{L/V_{ref}} \qquad \mu^* = \frac{\mu}{\mu_{ref}} \qquad \rho^* = \frac{\rho}{\rho_{ref}} \qquad P^* = \frac{P}{\rho_{ref} V_{ref}^2}$$

$$T^* = \frac{T}{T_{ref}} \qquad e^* = \frac{e}{V_{ref}^2} \qquad E_t^* = \rho^* \left(e^* + \frac{u_r^{*2} + u_z^{*2}}{2} \right)$$

$$\tag{44}$$

The non-dimensionalization procedure consists of substituting the above variables into Equations 33 through 43 , (PDE's + State). Below are the final form of the equations. The non-dimensional numbers that arise when this procedure is applied are:

Reynolds number: $Re = \dfrac{\rho_{ref} V_{ref} L}{\mu_{ref}}$

Prandtl number: $Pr = \dfrac{\nu}{a} = \dfrac{c_p \mu_{ref}}{k_{ref}}$

Eckert number: $Ec = \dfrac{c_p T_{ref}}{V_{ref}^2}$

Peclet number $Pe = RePr$

$$\beta = \dfrac{Lg}{V_{ref}^2}$$

C.3.1   Continuity equation

$$\frac{\partial \left(\rho^* r^*\right)}{\partial t^*} + \frac{\partial \left(\rho^* r^* u_r^*\right)}{\partial r^*} + \frac{\partial \left(\rho^* r^* u_z^*\right)}{\partial z^*} = 0 \tag{45}$$

C.3.2   r-Momentum equation

$$\frac{\partial \left(\rho^* r^* u_r^*\right)}{\partial t^*} + \frac{\partial}{\partial r^*} \left(\rho^* r^* u_r^{*2} - r^* \Pi_{rr}^*\right) + \frac{\partial}{\partial z^*} \left(\rho^* r^* u_r^* u_z^* - r^* \Pi_{rz}^*\right) =$$

$$\tag{46}$$

$$P^* - \frac{2}{3} \frac{\mu^*}{Re} \left(2 \frac{u_r^*}{r^*} - \frac{\partial u_r^*}{\partial r^*} - \frac{\partial u_z^*}{\partial z^*}\right)$$

C.3.3   z-Momentum equation

$$\frac{\partial \left(\rho^* r^* u_z^*\right)}{\partial t^*} + \frac{\partial}{\partial r^*} \left(\rho^* r^* u_r^* u_z^* - r^* \Pi_{rz}^*\right) + \frac{\partial}{\partial z^*} \left(\rho^* r^* u_z^{*2} - r^* \Pi_{zz}^*\right) = -\rho^* r^* \beta \tag{47}$$

C.3.4 Energy equation

$$\frac{\partial \left(r^* E_t^*\right)}{\partial t^*} + \frac{\partial \left(r^* E_t^* u_r^*\right)}{\partial r^*} + \frac{\partial \left(r^* E_t^* u_z^*\right)}{\partial z^*} =$$

$$\frac{Ec}{Pe} \left(\frac{\partial}{\partial r^*} \left(k^* r^* \frac{\partial T^*}{\partial r^*} \right) + \frac{\partial}{\partial z^*} \left(k^* r^* \frac{\partial T^*}{\partial z^*} \right) \right) \tag{48}$$

$$-\rho^* r^* \beta u_z^* + \frac{\partial}{\partial r^*} \left(r^* \left(\Pi_{rr}^* u_r^* + \Pi_{rz}^* u_z^* \right) \right) + \frac{\partial}{\partial z^*} \left(r^* \left(\Pi_{rz}^* u_r^* + \Pi_{zz}^* u_z^* \right) \right)$$

where

$$\Pi_{rr}^* = \left(-P^* + \frac{2}{3} \frac{\mu^*}{Re} \left(2 \frac{\partial u_r^*}{\partial r^*} - \frac{u_r^*}{r^*} - \frac{\partial u_z^*}{\partial z^*} \right) \right) \tag{49}$$

$$\Pi_{rz}^* = \frac{\mu^*}{Re} \left(\frac{\partial u_r^*}{\partial z^*} + \frac{\partial u_z^*}{\partial r^*} \right) \tag{50}$$

$$\Pi_{zz}^* = \left(-P^* + \frac{2}{3} \frac{\mu^*}{Re} \left(2 \frac{\partial u_z^*}{\partial z^*} - \frac{\partial u_r^*}{\partial r^*} - \frac{u_r^*}{r^*} \right) \right) \tag{51}$$

C.3.5 Equation of state

$$P^* = (\gamma - 1)\rho^* e^* \tag{52}$$

$$T^* = \frac{\gamma M_{ref}^2 P^*}{\rho^*} \tag{53}$$

where M_{ref} is the free stream Mach number $M_{ref} = \dfrac{V_{ref}}{\sqrt{\gamma R T_{ref}}}$.

The nondimensional form of the equations are identical (except for the asterisks and non-dimensional parameters) to the dimensional equations. For convenience the asterisks will be dropped from the nondimensional equations.

C.3.6 Variation of viscosity and thermal conductivity

Note that in the above equations μ^* and k^* are retained because these parameters vary with temperature. In the specifications of the model these values are expressed as functions of temperature as fitted from experimental data.

The viscosity of gases and most liquids increases slowly with pressure. Since the change in viscosity is only a few percent up to 100 atm (White (1986)),

pressure effects will be neglected for the purpose of this thesis. Gas viscosity increases with temperature; a common approximation is Sutherland's law:

$$\frac{\mu}{\mu_o} = \frac{\left(\dfrac{T}{T_o}\right)^{3/2}(T_o+S)}{T+S} \tag{54}$$

where μ_o is a known viscosity at a known absolute temperature T_o. For nitrogen at a temperature of $T_o = 491.6°$R, $\mu_o = 0.1663mP$ and $S \approx 192°$R. The constant S is fit to data, and accurate for a wide range of values, White (1986). For temperatures between 180°R and 2700°R (100K-1500K) the error associated with this approximation is $\pm2\%$, °R. The values for other gases are given in White (1974).

The conversion for temperature from °R to K is given by the relation $T(\text{K}) = T(°R)/1.8$ and for viscosity $1mP = 10^{-4}\,\dfrac{kg}{m \cdot s}$. Given these conversion relations Sutherland's law may be used as stated with $\mu_o = 0.1663 \times 10^{-4}\,\dfrac{kg}{m \cdot s}$, $T_o = 273.11K$, $S = 106.67K$ and T is the temperature in Kelvin. Note that the units of μ are now $\dfrac{kg}{m \cdot s}$.

Thermal conductivity is a thermodynamic property and varies with temperature and pressure as does viscosity. The conductivity is a function of the Prandtl number which is nearly constant for gases and equal to 0.72. From the definition of the Prandtl number: $k = \dfrac{c_p\mu}{Pr}$, where c_p is constant as given in the Equation of State and the viscosity μ as described above may be inserted here.

Further data on viscosity and conductivity can be found in Reid et al (1977).

C.4 Dimensional analysis

We can get a feeling of the relative importance of the different heat transfer phenomenon before solving the system of equations by doing a dimensional analysis of the equations. Thus it is important to follow the above by a description of the nondimensional parameters involved in this model. The following is a summary of nondimensional parameter groupings relevant to RTP, those given below with ranges were extracted from Rozemboom (1996). For further information on the origins of these non-dimensional parameters the reader is referred to White (1986).

Name	Definition	Description
Knudsen	$Kn = \dfrac{\lambda}{L}$	The Knudsen number represents the ratio of the mean free path λ to the charactersistic length L and is small for typical RTP conditions (Rozemboom(1996)), $Kn = \dfrac{\text{Mean free path}}{\text{Characteristic length}} < 0.01$ This implies that the continuum equations given above apply.
Prandtl	$Pr = \dfrac{\nu}{a}$	"The Prandtl number, the ratio of kinematic viscosity (ν) to thermal diffusivity (a), is nearly constant and equal to 0.7 for gases", Rozemboom(1996). $Pr = \dfrac{\text{Momentum diffusivity}}{\text{Thermal diffusivity}} = 0.7$
Reynolds	$Re = \dfrac{\rho_{ref} V_{ref} L}{\mu_{ref}}$	The Reynolds number represents the relative importance of the convection and viscosity of the fluid flow. $Re = \dfrac{\text{Inertial forces}}{\text{Viscous forces}}$ $\tilde{\ }1-100$ for laminar flows. Since the Reynolds number is less than 100 for RTP systems, this is an indication of laminar flow.
Peclet	$Pe = RePr$	The Peclet number represents the ratio of energy transport by convection to transfer by conduction $Pe = \dfrac{\text{Thermal flux by convection}}{\text{Thermal flux by diffusion}}$ $\tilde{\ }1-70$. Since $Pe > 1$ the heat transfer is dominated by convection.
	$\beta = \dfrac{Lg}{V_{ref}^2}$	β represents the ratio of gravitational force to inertial force. This can be seen by multiplying both the numerator and denominator by ρ_{ref}, $\beta = \dfrac{Lg}{V_{ref}^2}\dfrac{\rho_{ref}}{\rho_{ref}} = \dfrac{\text{mass}}{\text{pressure}}$

C.5 Boundary Conditions

For this model six different boundary conditions are needed. These are: Fixed Temperature, Wall Boundaries, Symmetry Boundaries, Inflow Boundaries, Outflow Boundaries and Radiation Boundaries. Most of these may be specified

by putting a constraint on the solution at the boundary of the computational domain. All the constraints will be written in terms of the nondimensional variables P, u_r, u_z, and T. For the generalized forms of the boundary constraints, the variables t and n are used for the tangential and normal directions at the boundary respectively. Some of the boundary constraints will be derived from the continuity and momentum equations.

C.5.1 Fixed Temperature Wall Boundaries

At a wall, a viscous fluid has velocity that matches the wall, and for all of the walls in the model being considered this velocity will be zero.

$$u_n = 0 \tag{55}$$

$$u_t = 0 \tag{56}$$

The walls that are considered in this model are water cooled and so maintained at a fixed temperature (isothermal), with exception of the radiating wafer which will be considered separately. The isothermal boundary constraint is to set the temperature to its constant value.

$$T = \text{CONSTANT} \tag{57}$$

A constraint on pressure at the wall can be derived from the momentum equations.

For the pressure constraint on a wall there are two possibilities given the domain of consideration. A wall surface that lies in the constant radius plane will be defined as a wall of constant radius. For a wall that is perpendicular to the first, we will define as a wall of constant z coordinate.

Wall of constant radius For walls at a constant radius we are interested in the r-momentum to derive a constraint on pressure. First we expand the momentum equation, discarding time derivatives since the boundary conditions do not change with time, then we insert the zero velocity conditions and combine with the continuity equation.

Expanding the r-momentum equation:

$$\frac{\partial}{\partial r}\left(\rho r u_r^2 - r\Pi_{rr}\right) + \frac{\partial}{\partial z}\left(\rho r u_r u_z - r\Pi_{rz}\right) = P - \frac{2}{3}\frac{\mu}{\text{Re}}\left(2\frac{u_r}{r} - \frac{\partial u_r}{\partial r} - \frac{\partial u_z}{\partial z}\right) \tag{58}$$

$$u_r^2 \frac{\partial(\rho r)}{\partial r} + \rho r 2 u_r \frac{\partial u_r}{\partial r} - r\frac{\partial \Pi_{rr}}{\partial r} - \Pi_{rr} + u_z \frac{\partial(\rho r u_r)}{\partial z} + \rho r u_r \frac{\partial u_z}{\partial z} - r\frac{\partial \Pi_{rz}}{\partial z} =$$

$$P - \frac{2}{3}\frac{\mu}{\text{Re}}\left(2\frac{u_r}{r} - \frac{\partial u_r}{\partial r} - \frac{\partial u_z}{\partial z}\right)$$

$$(59)$$

also expanding $\dfrac{\partial \Pi_{rr}}{\partial r}$ and $\dfrac{\partial \Pi_{rz}}{\partial z}$, since: $\Pi_{rr} = \left(-P + \dfrac{2}{3}\dfrac{\mu}{\text{Re}}\left(2\dfrac{\partial u_r}{\partial r} - \dfrac{u_r}{r} - \dfrac{\partial u_z}{\partial z}\right)\right)$
then:

$$\frac{\partial \Pi_{rr}}{\partial r} = \left(-\frac{\partial P}{\partial r} + \frac{2}{3}\frac{\mu}{\text{Re}}\left(2\frac{\partial^2 u_r}{\partial r^2} - \frac{1}{r}\frac{\partial u_r}{\partial r} + \frac{u_r}{r^2} - \frac{\partial^2 u_z}{\partial r \partial z}\right)\right) \qquad (60)$$

and since: $\Pi_{rz} = \dfrac{\mu}{\text{Re}}\left(\dfrac{\partial u_r}{\partial z} + \dfrac{\partial u_z}{\partial r}\right)$ then:

$$\frac{\partial \Pi_{rz}}{\partial z} = \frac{\mu}{\text{Re}}\left(\frac{\partial^2 u_r}{\partial z^2} + \frac{\partial^2 u_z}{\partial z \partial r}\right) \qquad (61)$$

now inserting the zero velocity boundary conditions leads to:

$$0 + 0 - r\left(-\frac{\partial P}{\partial r} + \frac{2}{3}\frac{\mu}{\text{Re}}\left(2\frac{\partial^2 u_r}{\partial r^2} - \frac{1}{r}\frac{\partial u_r}{\partial r} + 0 - \frac{\partial^2 u_z}{\partial r \partial z}\right)\right) - \left(-P + \frac{2}{3}\frac{\mu}{\text{Re}}\left(2\frac{\partial u_r}{\partial r} - 0 - \frac{\partial u_z}{\partial z}\right)\right)$$

$$+ 0 + 0 - r\frac{\mu}{\text{Re}}\left(\frac{\partial^2 u_r}{\partial z^2} + \frac{\partial^2 u_z}{\partial z \partial r}\right) = P - \frac{2}{3}\frac{\mu}{\text{Re}}\left(0 - \frac{\partial u_r}{\partial r} - \frac{\partial u_z}{\partial z}\right)$$

$$(62)$$

$$r\frac{\partial P}{\partial r} - \frac{4}{3}\frac{\mu}{\text{Re}}r\frac{\partial^2 u_r}{\partial r^2} + \frac{2}{3}\frac{\mu}{\text{Re}}\frac{\partial u_r}{\partial r} + \frac{2}{3}\frac{\mu}{\text{Re}}r\frac{\partial^2 u_z}{\partial r \partial z} + P - \frac{4}{3}\frac{\mu}{\text{Re}}\frac{\partial u_r}{\partial r} + \frac{2}{3}\frac{\mu}{\text{Re}}\frac{\partial u_z}{\partial z}$$

$$-r\frac{\mu}{\text{Re}}\frac{\partial^2 u_r}{\partial z^2} - r\frac{\mu}{\text{Re}}\frac{\partial^2 u_z}{\partial z \partial r} = P + \frac{2}{3}\frac{\mu}{\text{Re}}\frac{\partial u_r}{\partial r} + \frac{2}{3}\frac{\mu}{\text{Re}}\frac{\partial u_z}{\partial z}$$

$$(63)$$

and discarding the terms that cancel we obtain the equation:

$$r\frac{\partial P}{\partial r} - \frac{4}{3}\frac{\mu}{\text{Re}}r\frac{\partial^2 u_r}{\partial r^2} - \frac{4}{3}\frac{\mu}{\text{Re}}\frac{\partial u_r}{\partial r} - r\frac{\mu}{\text{Re}}\frac{\partial^2 u_r}{\partial z^2} - \frac{1}{3}r\frac{\mu}{\text{Re}}\frac{\partial^2 u_z}{\partial z \partial r} = 0 \qquad (64)$$

Since the wall is of constant radius any derivatives with respect to z are identically zero and may be discarded.

51

$$r\frac{\partial P}{\partial r} - \frac{4}{3}\frac{\mu}{\mathrm{Re}}r\frac{\partial^2 u_r}{\partial r^2} - \frac{4}{3}\frac{\mu}{\mathrm{Re}}\frac{\partial u_r}{\partial r} = 0 \tag{65}$$

Discarding z derivatives in the continuity equation and expanding:

$$\frac{\partial\left(\rho r u_r\right)}{\partial r} + \frac{\partial\left(\rho r u_z\right)}{\partial z} = 0 \tag{66}$$

$$\rho r\frac{\partial u_r}{\partial r} + u_r\left(\rho + r\frac{\partial\rho}{\partial r}\right) = 0 \tag{67}$$

Inserting zero velocity we are left with:

$$\rho r\frac{\partial u_r}{\partial r} = 0 \tag{68}$$

For non zero density and radius:

$$\frac{\partial u_r}{\partial r} = 0 \tag{69}$$

Combining this with the reduced momentum equation leads to:

$$\frac{\partial P}{\partial r} - \frac{4}{3}\frac{\mu}{\mathrm{Re}}\frac{\partial^2 u_r}{\partial r^2} = 0 \tag{70}$$

Finally leading to the pressure constraint:

$$\frac{\partial P}{\partial r} = \frac{4}{3}\frac{\mu}{\mathrm{Re}}\frac{\partial^2 u_r}{\partial r^2} \tag{71}$$

As discussed in the section on the variation of viscosity and thermal conductivity, μ is retained because it is a parameter that varies with temperature. The viscosity μ will be obtained using the information from the flux from the previous time step using a function called viscosity:

$$\mu = \mathrm{viscosity}(r, z) \tag{72}$$

Wall of constant z coordinate   Similarly, expanding the z-momentum equation:

$$\frac{\partial}{\partial r}\left(\rho r u_r u_z - r\Pi_{rz}\right) + \frac{\partial}{\partial z}\left(\rho r u_z^2 - r\Pi_{zz}\right) = -\rho r\beta \tag{73}$$

52

$$u_z \frac{\partial (\rho r u_r)}{\partial r} + \rho r u_r \frac{\partial u_z}{\partial r} - \Pi_{rz} - r \frac{\partial \Pi_{rz}}{\partial r} + u_z^2 \frac{\partial (\rho r)}{\partial z} + \rho r 2 u_z \frac{\partial u_z}{\partial z} - r \frac{\partial \Pi_{zz}}{\partial z} = -\rho r \beta$$

$$(74)$$

since: $\Pi_{zz} = \left(-P + \frac{2}{3} \frac{\mu}{Re} \left(2 \frac{\partial u_z}{\partial z} - \frac{\partial u_r}{\partial r} - \frac{u_r}{r} \right) \right)$ then:

$$\frac{\partial \Pi_{zz}}{\partial z} = \left(-\frac{\partial P}{\partial z} + \frac{2}{3} \frac{\mu}{Re} \left(2 \frac{\partial^2 u_z}{\partial z^2} - \frac{\partial^2 u_r}{\partial z \partial r} - \frac{1}{r} \frac{\partial u_r}{\partial z} \right) \right) \qquad (75)$$

and since: $\Pi_{rz} = \frac{\mu}{Re} \left(\frac{\partial u_r}{\partial z} + \frac{\partial u_z}{\partial r} \right)$ then:

$$\frac{\partial \Pi_{rz}}{\partial r} = \frac{\mu}{Re} \left(\frac{\partial^2 u_r}{\partial r \partial z} + \frac{\partial^2 u_z}{\partial r^2} \right) \qquad (76)$$

inserting the zero velocity boundary conditions leads to:

$$0 + 0 - \frac{\mu}{Re} \left(\frac{\partial u_r}{\partial z} + \frac{\partial u_z}{\partial r} \right) - r \frac{\mu}{Re} \left(\frac{\partial^2 u_r}{\partial r \partial z} + \frac{\partial^2 u_z}{\partial r^2} \right) + 0 + 0$$

$$-r \left(-\frac{\partial P}{\partial z} + \frac{2}{3} \frac{\mu}{Re} \left(2 \frac{\partial^2 u_z}{\partial z^2} - \frac{\partial^2 u_r}{\partial z \partial r} - \frac{1}{r} \frac{\partial u_r}{\partial z} \right) \right) = -\rho r \beta$$

$$(77)$$

$$-\frac{\mu}{Re} \frac{\partial u_r}{\partial z} - \frac{\mu}{Re} \frac{\partial u_z}{\partial r} - r \frac{\mu}{Re} \frac{\partial^2 u_r}{\partial r \partial z} - r \frac{\mu}{Re} \frac{\partial^2 u_z}{\partial r^2} + r \frac{\partial P}{\partial z} - \frac{4}{3} \frac{\mu}{Re} r \frac{\partial^2 u_z}{\partial z^2} + \frac{2}{3} \frac{\mu}{Re} r \frac{\partial^2 u_r}{\partial z \partial r}$$

$$+ \frac{2}{3} \frac{\mu}{Re} \frac{\partial u_r}{\partial z} = -\rho r \beta$$

$$(78)$$

discarding the terms that cancel leads to:

$$-\frac{1}{3} \frac{\mu}{Re} \frac{\partial u_r}{\partial z} - \frac{\mu}{Re} \frac{\partial u_z}{\partial r} - r \frac{\mu}{Re} \frac{1}{3} \frac{\partial^2 u_r}{\partial r \partial z} - r \frac{\mu}{Re} \frac{\partial^2 u_z}{\partial r^2} + r \frac{\partial P}{\partial z} - \frac{4}{3} \frac{\mu}{Re} r \frac{\partial^2 u_z}{\partial z^2} = -\rho r \beta$$

$$(79)$$

Since the surface has a constant z coordinate, and there is no radial variation,

all radial derivatives are discarded:

$$-\frac{1}{3} \frac{\mu}{Re} \frac{\partial u_r}{\partial z} + r \frac{\partial P}{\partial z} - \frac{4}{3} \frac{\mu}{Re} r \frac{\partial^2 u_z}{\partial z^2} = -\rho r \beta \qquad (80)$$

53

Expanding the continuity equation:

$$\frac{\partial \left(\rho r u_r \right)}{\partial r} + \frac{\partial \left(\rho r u_z \right)}{\partial z} = 0 \tag{81}$$

$$\rho r \frac{\partial u_r}{\partial r} + u_r \left(\rho + r \frac{\partial \rho}{\partial r} \right) + \rho r \frac{\partial u_z}{\partial z} + u_z \frac{\partial \left(\rho r \right)}{\partial z} = 0 \tag{82}$$

Taking derivatives of the equation with respect to z:

$$\rho r \frac{\partial^2 u_r}{\partial z \partial r} + \frac{\partial u_r}{\partial r} \frac{\partial \left(\rho r \right)}{\partial z} + \frac{\partial u_r}{\partial z} \left(\rho + r \frac{\partial \rho}{\partial r} \right) + u_r \left(\frac{\partial \rho}{\partial z} + r \frac{\partial^2 \rho}{\partial z \partial r} \right)$$

$$+ \rho r \frac{\partial^2 u_z}{\partial z^2} + \frac{\partial u_z}{\partial z} \frac{\partial \left(\rho r \right)}{\partial z} + u_z \frac{\partial^2 \left(\rho r \right)}{\partial z^2} + \frac{\partial u_z}{\partial z} \frac{\partial \left(\rho r \right)}{\partial z} = 0 \tag{83}$$

Inserting zero velocity and discarding derivatives with respect to r we are left

with:

$$\rho \frac{\partial u_r}{\partial z} + \rho r \frac{\partial^2 u_z}{\partial z^2} + 2 \frac{\partial u_z}{\partial z} \frac{\partial \left(\rho r \right)}{\partial z} = 0 \tag{84}$$

For non zero density and radius:

$$\frac{\partial u_r}{\partial z} = -r \frac{\partial^2 u_z}{\partial z^2} - 2 \frac{1}{\rho} \frac{\partial u_z}{\partial z} \frac{\partial \left(\rho r \right)}{\partial z} \tag{85}$$

Using the expanded continuity equation:

$$\rho r \frac{\partial u_r}{\partial r} + u_r \left(\rho + r \frac{\partial \rho}{\partial r} \right) + \rho r \frac{\partial u_z}{\partial z} + u_z \frac{\partial \left(\rho r \right)}{\partial z} = 0 \tag{86}$$

when the zero velocities and r derivatives are discarded we obtain:

$$\rho r \frac{\partial u_z}{\partial z} = 0 \tag{87}$$

and for non zero density and radius:

$$\frac{\partial u_z}{\partial z} = 0 \tag{88}$$

54

inserting this into the previous result from the continuity equation:

$$\frac{\partial u_r}{\partial z} = -r\frac{\partial^2 u_z}{\partial z^2} \tag{89}$$

Combining this with the reduced momentum equation leads to:

$$-\frac{1}{3}\frac{\mu}{\mathrm{Re}}\left(-r\frac{\partial^2 u_z}{\partial z^2}\right) + r\frac{\partial P}{\partial z} - \frac{4}{3}\frac{\mu}{\mathrm{Re}}r\frac{\partial^2 u_z}{\partial z^2} = -\rho r\beta \tag{90}$$

Finally leading to the pressure constraint:

$$\frac{\partial P}{\partial z} = \frac{\mu}{\mathrm{Re}}\frac{\partial^2 u_z}{\partial z^2} - \rho\beta \tag{91}$$

The density ρ will be obtained using the information from the flux from the previous time step using a function called density:

$$\rho = \mathrm{density}(r, z) \tag{92}$$

and the viscosity μ will be obtained using the information from the flux from the previous time step using a function called viscosity:

$$\mu = \mathrm{viscosity}(r, z) \tag{93}$$

C.5.2 Symmetry Boundaries

In the case of symmetry, the velocity normal to the boundary is constrained to be zero.

$$u_n = 0 \tag{94}$$

The tangential velocity, temperature and pressure are constrained to have no variation perpendicular to the boundary.

$$\frac{\partial u_t}{\partial n} = 0 \tag{95}$$

$$\frac{\partial T}{\partial n} = 0 \tag{96}$$

$$\frac{\partial P}{\partial n} = 0 \tag{97}$$

C.5.3 Inflow Boundaries

The inflow boundaries in this model have a constant z coordinate. The velocity profile at inflow boundaries is assumed fully-developed, ($\dfrac{\partial u_n}{\partial n} = 0$), correspondingly the input profile of velocity normal to the boundary is specified and the tangential component of velocity is constrained to be zero.

$$u_z = \text{InflowVel}(r) \tag{98}$$

$$u_r = 0 \tag{99}$$

The temperature of the fluid before it enters the chamber is a specified constant, and so the temperature at the inflow is constrained to the specified fixed temperature.

$$T = \text{CONSTANT} \tag{100}$$

The pressure constraint is derived from the continuity and z-momentum equations along with the conditions of fully-developed flow ($\dfrac{\partial u_z}{\partial z} = 0$). Expanding the z-momentum equation:

$$\frac{\partial}{\partial r}\left(\rho r u_r u_z - r\Pi_{rz}\right) + \frac{\partial}{\partial z}\left(\rho r u_z^2 - r\Pi_{zz}\right) = -\rho r\beta \tag{101}$$

$$u_z\frac{\partial\left(\rho r u_r\right)}{\partial r} + \rho r u_r\frac{\partial u_z}{\partial r} - \Pi_{rz} - r\frac{\partial\Pi_{rz}}{\partial r} + u_z^2\frac{\partial\left(\rho r\right)}{\partial z} + \rho r 2 u_z\frac{\partial u_z}{\partial z} - r\frac{\partial\Pi_{zz}}{\partial z} = -\rho r\beta \tag{102}$$

since: $\Pi_{zz} = \left(-P + \dfrac{2}{3}\dfrac{\mu}{\text{Re}}\left(2\dfrac{\partial u_z}{\partial z} - \dfrac{\partial u_r}{\partial r} - \dfrac{u_r}{r}\right)\right)$ then:

$$\frac{\partial\Pi_{zz}}{\partial z} = \left(-\frac{\partial P}{\partial z} + \frac{2}{3}\frac{\mu}{\text{Re}}\left(2\frac{\partial^2 u_z}{\partial z^2} - \frac{\partial^2 u_r}{\partial z\partial r} - \frac{1}{r}\frac{\partial u_r}{\partial z}\right)\right) \tag{103}$$

and since: $\Pi_{rz} = \dfrac{\mu}{\text{Re}}\left(\dfrac{\partial u_r}{\partial z} + \dfrac{\partial u_z}{\partial r}\right)$ then:

$$\frac{\partial\Pi_{rz}}{\partial r} = \frac{\mu}{\text{Re}}\left(\frac{\partial^2 u_r}{\partial r\partial z} + \frac{\partial^2 u_z}{\partial r^2}\right) \tag{104}$$

now inserting the fully developed boundary conditions leads to:

$$u_z\frac{\partial\left(\rho r u_r\right)}{\partial r} + 0 - \frac{\mu}{\text{Re}}\left(\frac{\partial u_r}{\partial z} + \frac{\partial u_z}{\partial r}\right) - r\frac{\mu}{\text{Re}}\left(\frac{\partial^2 u_r}{\partial r\partial z} + \frac{\partial^2 u_z}{\partial r^2}\right) + u_z^2\frac{\partial\left(\rho r\right)}{\partial z}$$

$$+0 - r\left(-\frac{\partial P}{\partial z} + \frac{2}{3}\frac{\mu}{\text{Re}}\left(0 - \frac{\partial^2 u_r}{\partial z\partial r} - \frac{1}{r}\frac{\partial u_r}{\partial z}\right)\right) = -\rho r\beta \tag{105}$$

$$u_z \frac{\partial (\rho r u_r)}{\partial r} - \frac{\mu}{Re}\frac{\partial u_r}{\partial z} - \frac{\mu}{Re}\frac{\partial u_z}{\partial r} - r\frac{\mu}{Re}\frac{\partial^2 u_r}{\partial r \partial z} - r\frac{\mu}{Re}\frac{\partial^2 u_z}{\partial r^2} + u_z^2 \frac{\partial (\rho r)}{\partial z}$$

$$+r\frac{\partial P}{\partial z} + r\frac{2}{3}\frac{\mu}{Re}\frac{\partial^2 u_r}{\partial z \partial r} + \frac{2}{3}\frac{\mu}{Re}\frac{\partial u_r}{\partial z} = -\rho r \beta \tag{106}$$

Since the inflows have a constant z coordinate, radial derivatives are discarded:

$$u_z^2 \frac{\partial (\rho r)}{\partial z} + r\frac{\partial P}{\partial z} - \frac{1}{3}\frac{\mu}{Re}\frac{\partial u_r}{\partial z} = -\rho r \beta \tag{107}$$

Expanding the continuity equation:

$$\frac{\partial (\rho r u_r)}{\partial r} + \frac{\partial (\rho r u_z)}{\partial z} = 0 \tag{108}$$

$$\rho r \frac{\partial u_r}{\partial r} + u_r \left(\rho + r\frac{\partial \rho}{\partial r} \right) + \rho r \frac{\partial u_z}{\partial z} + u_z \frac{\partial (\rho r)}{\partial z} = 0 \tag{109}$$

Inserting the fully developed boundary conditions and discarding derivatives with respect to r, in the continuity equation, we are left with:

$$u_z \frac{\partial (\rho r)}{\partial z} = 0 \tag{110}$$

For non-zero u_z:

$$\frac{\partial (\rho r)}{\partial z} = 0 \tag{111}$$

The resultant constraint on pressure becomes:

$$\frac{\partial P}{\partial z} = -\rho \beta + \frac{1}{3}\frac{1}{r}\frac{\mu}{Re}\frac{\partial u_r}{\partial z} \tag{112}$$

From the expanded form of the continuity equation:

$$\rho r \frac{\partial u_r}{\partial r} + u_r \left(\rho + r\frac{\partial \rho}{\partial r} \right) + \rho r \frac{\partial u_z}{\partial z} + u_z \frac{\partial (\rho r)}{\partial z} = 0 \tag{113}$$

Taking derivatives of the equation with respect to z:

$$\rho r \frac{\partial^2 u_r}{\partial z \partial r} + \frac{\partial u_r}{\partial r}\frac{\partial (\rho r)}{\partial z} + \frac{\partial u_r}{\partial z}\left(\rho + r\frac{\partial \rho}{\partial r} \right) + u_r \left(\frac{\partial \rho}{\partial z} + r\frac{\partial^2 \rho}{\partial z \partial r} \right)$$

$$+\rho r \frac{\partial^2 u_z}{\partial z^2} + \frac{\partial u_z}{\partial z}\frac{\partial (\rho r)}{\partial z} + u_z \frac{\partial^2 (\rho r)}{\partial z^2} + \frac{\partial u_z}{\partial z}\frac{\partial (\rho r)}{\partial z} = 0 \tag{114}$$

Inserting the fully developed boundary conditions and discarding derivatives with respect to r we are left with:

$$\rho \frac{\partial u_r}{\partial z} = -u_z r \frac{\partial^2 \rho}{\partial z^2} \tag{115}$$

Inserting this into the reduced momentum equation leads to the constraint on pressure:

$$\frac{\partial P}{\partial z} = -\rho \beta - \frac{1}{3\rho} u_z \frac{\mu}{\text{Re}} \frac{\partial^2 \rho}{\partial z^2} \tag{116}$$

The density ρ will be obtained using the information from the flux from the previous time step using the function called density:

$$\rho = \text{density}(r, z) \tag{117}$$

and the viscosity μ will be obtained using the information from the flux from the previous time step using the function called viscosity:

$$\mu = \text{viscosity}(r, z) \tag{118}$$

C.5.4 Outflow Boundaries

At the ouflow, the velocities and temperature will be assumed to be fully developed. Correspondingly the temperature and the normal velocity does not change normal to the boundary, and the tangential component of velocity is constrained to be zero.

$$\frac{\partial T}{\partial n} = 0 \tag{119}$$

$$\frac{\partial u_n}{\partial n} = 0 \tag{120}$$

$$u_t = 0 \tag{121}$$

Since the pressure outside the chamber is known, the pressure at the outflow boundary is constrained to be the specified fixed value.

$$P = \text{CONSTANT} \tag{122}$$

C.5.5 Radiation Boundaries

The only boundary which will require the radiation boundary condition is the wafer boundary, which is a fixed wall, and thus the velocities are set to zero.

$$u_r = 0 \tag{123}$$

$$u_n = 0 \tag{124}$$

A constraint on pressure at the wall can be derived from the continuity and

momentum equations as was done for the Fixed Temperature Wall Boundaries and since the radiation boundary is on a surface with constant z coordinate the resulting pressure constraint is given by:

$$\frac{\partial P}{\partial z} = \frac{\mu}{\text{Re}} \frac{\partial^2 u_z}{\partial z^2} - \rho\beta \tag{125}$$

The density ρ will be obtained using the information from the flux from the previous time step using the function called density:

$$\rho = \text{density}(r, z) \tag{126}$$

and the viscosity μ will be obtained using the information from the flux from the previous time step using the function called viscosity:

$$\mu = \text{viscosity}(r, z) \tag{127}$$

The unique part of this boundary condition is the constraint on temperature. At each step in time the heat balance equation is solved on the wafer using the radiation model of this thesis, producing a time varying temperature profile at the surface of the wafer.

$$T = T(r, t^*) \tag{128}$$

where t^* denotes time.

Once the temperature profile is calculated the values may be inserted as a fixed temperature boundary condition for the fluid problem by assigning the constraint above. Then one solves the fluid problem for one step in time and achieves a temperature and flow profile inside the chamber. Once this has been attained the information is used to get the temperature gradient above the wafer. One inserts this into the heat balance equation and then advances the temperature on the wafer by one time step. Then we return to the fluid problem for one time step and so forth for the full process run which should achieve a transient solution which includes the effects of a gas flow in the chamber.

D Input data

This appendix contains information about silicon and nitrogen that were needed to do the present study of temperature on the silicon wafer. The first and second section discuss the Specific Heat and Density of silicon and a data table is used for these variables. The third and fourth sections discuss the viscosity and thermal conductivity of nitrogen. The viscosity of nitrogen is derived from Sutherland's law and the conductivity of nitrogen is derived using the definition of the Prandtl number which in practice is constant for gases.

D.1 Specific Heat of silicon

The Specific heat of silicon varies greatly for the temperatures ranges considered in the RTP process run, so the values used have been extracted from data tables in the "Materials Handbook", Brady (1972).

Specific Heat:

Temperature, K	Specific heat, $J/(kg \cdot K)$
60	115
100	259
200	557
300	713
400	785
500	832
600	849
700	866
800	883
900	899
1000	916
1100	933
1200	950
1300	967
1400	983
1500	1000

D.2 Density of silicon

The variation of density with temperature does not vary as significantly as a function of temperature as the heat capacity does; however included in the model are the values extracted from the "Materials Handbook", Brady (1972).

Density:

Temperature, K	Density, kg/m^3
298	2329
400	....................2326.9
700	....................2319.2
900	....................2313.6
1100	....................2307.7
1300	....................2301.6

D.3 Viscosity of nitrogen

"The viscosity of gases and most liquids increases slowly with pressure. Since the change in viscosity is only a few percent up to 100 atm," White (1986), pressure effects will be neglected for the purpose of this thesis. Gas viscosity increases with temperature; a common approximation and what is used in the model of this thesis is Sutherland's law:

$$\frac{\mu}{\mu_o} = \frac{\left(\frac{T}{T_o}\right)^{3/2}(T_o + S)}{T + S} \tag{129}$$

where μ_o is a known viscosity at a known absolute temperature T_o. For nitrogen at a temperature of $T_o = 273.11K$, $\mu_o = 0.1663mP = 0.1663 \times 10^{-4}\ \frac{kg}{m \cdot s}$ and $S = 106.67K$. The constant S is fit to data, and accurate for a wide range of values. "For temperatures between 180°R and 2700°R (100K-1500K) the error associated with this approximation is $\pm 2\%$," White (1986). The values for other gases are given in White (1974).

D.4 Thermal Conductivity of nitrogen

Thermal conductivity is a thermodynamic property and varies with temperature and pressure as does viscosity. The conductivity is a function of the Prandtl number which is nearly constant for gases and equal to 0.72. From the definition of the Prandtl number: $Pr = \frac{c_p\mu}{k}$, solving for k leads to: $k = \frac{c_p\mu}{Pr}$, where $c_p = \frac{\gamma R}{\gamma - 1}$ and R is the gas constant and has a value of 296.8 for nitrogen. γ is the ratio of the specific heats. The following is a table of some sample values at atmospheric pressure of the specific heats at the high temperatures we are considering. These values are extracted from the CRC "Handbook of Chemistry and Physics," Lide(1993).

Temperature, K	c_v, $J/(mol \cdot K)$	c_p, $J/(mol \cdot K)$
800	23.1	31.4
900	23.7	32.0
1000	24.3	32.6

Taking the ratio of the specific heats results in a value for γ of approximately 1.35 at these temperatures. The viscosity μ as described above may be inserted here to obtain the conductivity k. Further data on viscosity and conductivity can be found in Reid et al (1977).

D.5 Temperature gradients

The temperature gradient above and below the wafer are needed in order to solve the heat balance equation, and so a linear approximation to this is used for this study. Above the wafer let the distance between the wafer and the showerhead be: d_{aw}. At a time t^* the heat gradient at the ith ring above the wafer is given by the temperature difference between the constant temperature of the showerhead: T_{sh} and the temperature at the ith ring: $T_i(t^*)$, divided by d_{aw}.

$$\frac{\partial T}{\partial y}_{aw} = \frac{T_i(t^*) - T_{sh}}{d_{aw}}$$

Below the wafer the distance between the wafer and the bottom of the chamber is 18 inches, and so in SI units: $d_{bw} = 0.4572m$. At a time t^* the heat gradient at the ith ring below the wafer is given by the temperature difference between the constant temperature of the chamber bottom: T_{cb} and the temperature at the ith ring: $T_i(t^*)$, divided by d_{bw}

$$\frac{\partial T}{\partial y}_{bw} = \frac{T_i(t^*) - T_{cb}}{0.4572}$$